



TECHNISCHE  
UNIVERSITÄT  
WIEN  
Vienna University of Technology

## MASTER-THESIS

# Impact of Temperature and Temperature-Change on Range-Cameras

Accomplished at the Institute of  
**Photogrammetry and Remote Sensing**  
Vienna University of Technology

Examiner: Univ.Prof. Dipl.-Ing. Dr.techn. Norbert Pfeifer  
Supervisor: Projektass. Dipl.-Ing. Wilfried Karel

in cooperation with the Institute of  
**Geodesy and Geophysics**  
Vienna University of Technology

with support of  
Univ.Prof. Dipl.-Ing. Dr.techn. Andreas Wieser  
and Univ.Ass. Dipl.-Ing. Stefan Lederbauer

by  
Philipp Zachhuber  
Eduard-Bach-Straße 2a  
4540 Bad Hall

Vienna, September 21<sup>st</sup> 2011 \_\_\_\_\_

# Acknowledgements

I would like to thank all those People who made it possible for me to write this thesis:

PAUL BERLINGER from the “*Institute of Applied Physics*” for his advice and the construction of an Infra-red sensor.

PAUL BRANDL from the “*Institute of Electrodynamics, Microwave and Circuit Engineering*” (EMCE) for a very helpful introduction to the use of the Oscilloscope and for the supply of other electrotechnical equipment.

CLAUDIA EDER, JOHANNES FABIANKOWITSCH, STEFAN LEDERBAUER and ANDREAS WIESER from the “*Institute of Geodesy and Geophysics*” for their help and support from ordering and funding equipment over organising the measurement laboratory to the set up of the linux software for the CamCube and their involvement in various meetings.

WILFRIED KAREL, NORBERT PFEIFER and HANS THÜMINGER from the “*Institute of Photogrammetry and Remote Sensing*” (IPF) for their help with components, the IPF-Software and helpful discussions and pieces of advice.

GEORG RAMER and BERNHARD ZACHHUBER from the “*Institute of Chemical Technologies and Analytics*” for placing their infrared-camera at my dispose.

At this point I would like to thank the “Vienna University of Technology” for the great variety of institutes with utterly helpful staff.

GEORG, JOHANNA D.G. and ULRIKE for certain instruments, FRANZI for proofreading and the fourth floor and other residents of a famous student housing for making the years there to such a great time. Especially ALEX and MIMI deserve to be mentioned separately for reasons they know.

Finally I should not forget EVA, RESI, SIMON and all other mates from the university who provided a pleasant study-environment.

Mein besonderer Dank geht an meine Eltern, die mir das Studium ermöglicht haben und mich in jeder Hinsicht unterstützt haben.

## **Abstract**

The present master thesis deals with the various influences of temperature on range cameras.

The influences on the measured data and on the electronics itself as well as the relation between integration time and internal temperature was investigated. Experiments were carried out with permanent monitoring of the housing temperature or if available the internal one was used.

Measured distances as well as amplitudes were found to be depending on temperature with increasing distances and decreasing amplitudes at higher temperatures. Moreover the sensor's temperature of the SwissRanger 3000 was found to increase with longer integration times.

A look at dark current in the sensors revealed a quadratic increase of the amplitudes with temperature and a spatial dependence. Furthermore the stability of the sensor and the camera housing was investigated and showed some room for improvements.

## **Zusammenfassung**

Die vorliegende Masterarbeit behandelt unterschiedliche Einflüsse von Temperatur auf Distanzkameras.

Sowohl Einflüsse auf Messdaten und Elektronik wurden nebst dem Zusammenhang zwischen Integrationszeit und interner Temperatur untersucht. Dazu wurden Gehäuse- und interne Temperaturen durchgehend überwacht soweit dies möglich war.

Mit steigender Temperatur wurden größere Distanzen und kleinere Amplituden registriert. Eine höhere Sensortemperatur bei längerer Integrationszeit wurde beim SwissRanger 3000 festgestellt.

Dunkelstrom im Sensor zeigte einen quadratischen Anstieg mit steigender Temperatur und auch eine Abhängigkeit von der Position des Pixels. Bei der Formstabilität des Sensors selber und vor allem des Gehäuses wurde Raum für Verbesserungen ausgemacht.

# Contents

<b>1</b>	<b>Introduction</b>	<b>1</b>
1.1	Motivation . . . . .	1
1.2	Related Work . . . . .	2
1.3	Aim of this Thesis . . . . .	3
<b>2</b>	<b>Range Imaging Cameras</b>	<b>4</b>
2.1	Functionality of Range Imaging Cameras . . . . .	4
2.1.1	Time-of-Flight Measurement Principle . . . . .	4
2.1.2	Phase-Difference Distance Measurement . . . . .	5
2.1.3	Implementation . . . . .	5
2.2	Range Imaging Cameras for Testing . . . . .	6
2.2.1	The Image Sensors . . . . .	6
2.2.2	The Illumination . . . . .	8
2.2.3	The Cooling System . . . . .	11
2.2.4	Overview of Features of the Cameras . . . . .	13
<b>3</b>	<b>Considerations on Setup</b>	<b>14</b>
3.1	Geometry of the Object Space . . . . .	14
3.1.1	Geometry of the Target . . . . .	14
3.1.2	Target Distance . . . . .	15
3.2	Camera mounting . . . . .	16
3.2.1	Temperature Tapping . . . . .	17
3.2.2	Camera Support . . . . .	17
3.3	Ambient Light . . . . .	19
3.4	Ambient Temperature . . . . .	20
<b>4</b>	<b>Methods</b>	<b>22</b>
4.1	Data Acquisition . . . . .	22
4.2	Experiments . . . . .	22
4.2.1	Determination of the Target positions . . . . .	23
4.2.2	Differences in Dark Current distribution . . . . .	24
<b>5</b>	<b>Results</b>	<b>25</b>

5.1	Influence on Measured Data . . . . .	25
5.1.1	Permanence at Room Temperature . . . . .	25
5.1.2	Influence on Distance . . . . .	28
5.1.3	Influence on Amplitude . . . . .	32
5.2	Influence of the integration time on internal temperature . . . . .	34
5.3	Influence of Temperature on the Electronics . . . . .	36
5.3.1	Dark Current in the Sensor . . . . .	36
5.3.2	Geometric stability of the imaging sensor . . . . .	39
5.3.3	Sensor-location dependence of dark current . . . . .	43
5.3.4	Influence on the active Illumination . . . . .	45
5.3.5	Frequency Stability of the Illumination . . . . .	47
5.4	Summary of Results . . . . .	50
<b>6</b>	<b>Conclusion</b>	<b>51</b>
6.1	Conclusions . . . . .	51
6.2	Temperature related recommendations for practical work . . . . .	52
6.3	Future Work . . . . .	52
<b>A</b>	<b>Appendix</b>	<b>53</b>
A.1	Instruments used for Experiments . . . . .	53
A.1.1	Devices for heating and cooling . . . . .	53
A.1.2	Temperature Loggers . . . . .	54
A.1.3	Instruments for Illumination Analysis . . . . .	54
	<b>Bibliography</b>	<b>57</b>

# 1 Introduction

## 1.1 Motivation

The initial motivation to write about Range Imaging Cameras (RIMs) was the possibility to contribute to the enhancement of the navigation capabilities of the partly internal project of a 4-wheel robot (Seekur Jr.) that is currently under active development at the “*Institute of Geodesy and Geophysics*”. This vehicle is used for developing and testing navigation algorithms. One essential part of it, besides the GPS receivers and radio antennas, is a range-camera, the CamCube 2.0 from PMDtech (CamCube). This range camera is used for kinematic position determination. The final device should allow precise navigation without further external guidance like a tracking total station.

It turned out that also the “*Institute of Photogrammetry and Remote Sensing*” (IPF) is connected to research around RIMs. They have the much smaller SwissRanger 3000 (SR3000) and were investigating internal scattering effects at the beginning of this work. There might be a more detailed research in this thesis about the SR3000 simply because of the easier handling, quicker data processing and the fact that it is not as bulky and can be brought to intended temperatures in a reasonable time. Nevertheless the main experiments were carried out with both cameras, of course.

The fact that the influences of temperature have not been thoroughly researched so far made it very challenging to work on this topic. Statements like “*Measurements are found to be highly dependent on temperature, and on the illumination and reflectivity of the objects.*” (Pattinson, 2010) made it even more interesting to fill this gap. PATTINSON also states that frequency-dependent calibration parameters would be no longer valid if the frequency they are based on is no longer static because of dependence on temperature.

More encouraging statements were given by other researchers for example “*... temperature-induced drifts of the distance measurement lead to significant errors.*” (Kahlmann, 2007) and “*It is a known fact that the depth measurement drifts with the camera’s temperature. It is yet to be properly investigated how this error behaves systematically with temperature.*” (Rapp, 2007). Those drifts could be detected and the findings hopefully improve the understanding on this topic.

Finally I want to cite some more cognitions that even more directed my interest to temperature related investigations: “*...temperature effects are one of the dominant*

*influences in range imaging.” ... “... the reduction of uncontrolled temperature effects will become more important” (Kahlmann, 2007)*

## 1.2 Related Work

The first successful realisation of an all-solid-state 3D Time-of-Flight (ToF) range-camera is described in Lange (2000). Aside from hardware related chapters mostly focusing on the usability of different types of components also thermal effects like the diffusion of charges and temperature-variable characteristics related to the control current of the illuminating LEDs are mentioned. A recommendation for operating imagers at low temperatures is given. In the succeeding publication by Lange and Seitz (2001) the focus is, among others subjects, kept on the power budget and thermal diffusion and thermal noise (dark current).

Also an interesting work related to range-cameras and the importance of the dependence of modulators on temperature was carried out by Heinol (2001). His work deals mostly with new modulation concepts.

In the following time attention was drawn to the internal heating of instruments and to distance drifts as a consequence thereof (Luan, 2001) but also detailed investigation of influences on the electronics were carried out (e.g. Schneider (2003)). Later on a group around KAHLMANN started more detailed research on thermal effects (Kahlmann, Remondino, and Ingensand, 2006) which also plays a role in his dissertation (Kahlmann, 2007) where he notes a higher distance reading at higher ambient temperatures and introduces a constructional correction by an internal reference path which reduces the temperature influence during the warming up phase down to around 20 %. Experiments similar to the ones carried out within my present work can be found in KAHLMANN’s works too but only ambient temperatures are used there which do not seem to be directly related to effects in the recorded data. Nevertheless he uses a closed temperature cycle and different behaviour can be interpreted into the results.

Finally I must not forget to mention more recent researches like from Steiger, Felder, and Weiss (2008) or Pattinson (2010) with sections about various influences of temperature. Also the ongoing research on optoelectronic integrated circuits (OEICs) at the EMCE<sup>1</sup> should be mentioned (e.g. the ongoing Thesis “*Untersuchung eines Referenzkanals für einen 3D Kamera Chip*” by MICHAEL HOFBAUER or work by Zach, Davidovic, and Zimmermann (2010))

---

<sup>1</sup><http://www.emce.tuwien.ac.at/en/index.htm>

### **1.3 Aim of this Thesis**

The aim of this thesis is to further investigate thermal effects on RIMs. In contrast to the publications mentioned before, the idea behind this work is to focus on effects caused by temperature only. That way a better understanding of the effect of internal, external and other temperatures should be achieved. Sufficient experiments should back up the findings and allow precise recommendations on the use of RIMs at certain temperatures or changing environments.

Influences of the atmosphere's temperature were found to be not relevant (Kahlmann, 2007) in most cases and are not of interest for this work.

Especially the period of acclimatisation, due to changing ambient temperatures, is of great interest because this is the period of major changes in the recorded data. The beginning of recording was also problematic to handle in other publications because of sometimes erratic measurements after switching on the instrument.

Two different range cameras were available. A look at the components of those cameras is taken after an introduction into basic range imaging principles. The results are presented after the chapters on the set-up of the experiments and methods used. Finally, conclusions are made and recommendations for future works are given.



## 2 Range Imaging Cameras

*“A range image is a large collection of distance measurements from a known reference coordinate system to surfacepoints on object(s) in a scene.”* Besl (1988)

### 2.1 Functionality of Range Imaging Cameras

According to Besl (1988) Range Imaging Cameras belong to the category of field-of-view sensors as they deliver instantly a distance image of all visible points without any movement of the sensor or any other part of the camera. It should be kept in mind that a representation of distances in a regular grid might be called range image regardless of how the data was collected which can be misleading.

The following two subsections should only give a glimpse of two measurement principles. The basic ideas are depicted in Figure 2.1. More detailed descriptions can be found in numerous references mentioned in Chapter 1.2.

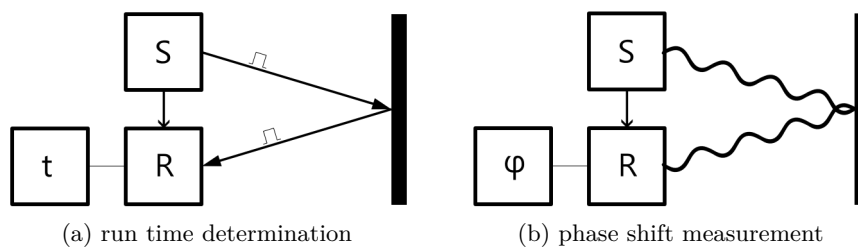


Figure 2.1: Overview of distance measurement principles.

#### 2.1.1 Time-of-Flight Measurement Principle

The Time-of-Flight principle is based on the fact that light travels at a certain limited speed. The period of a light pulse from the point of sending to the point of receiving is therefore used to calculate the distance. In the common case that sender and receiver are at the same location, formula (2.1) gives the object distance:

$$v = \frac{2d}{t} \Rightarrow d = \frac{ct}{2}, \quad (2.1)$$

with  $v$  and  $c$  standing for velocity and speed of light while  $d$  and  $t$  describe distance and time.

The introduction of Lange (2000) gives a good summary on this topic with interesting historical background information. In Karel (2007) an overview of pulsed systems is given.

### 2.1.2 Phase-Difference Distance Measurement

This measurement principle is using the wavelength of an modulated light wave. The phase shift  $\varphi$  of the reflected signal is used to calculate the distance. Possible ambiguities can be solved by using more than just one wavelength or by algorithms carrying out a phase unwrapping.

### 2.1.3 Implementation

The cameras used in this work are based on the determination of the distance by using the measurement of phase-differences. Using an active illumination with a certain amplitude modulation of the used infra red light the reflected signal is then received at the sensor and usually sampled at four points to reconstruct the phase angle  $\varphi$  of the reflected signal.

Using a modulation frequency of 20 MHz which both cameras have in common and are used throughout most other publications gives an unambiguous range<sup>1</sup>  $d_{max} = \frac{c}{2f_{mod}}$  of 7.49 m The distance itself is derived from equation (2.2) using the phase offset  $\varphi$  of the received signal.

$$d = \frac{\lambda_{mod}}{2} \frac{\varphi}{2\pi} \quad (2.2)$$

---

<sup>1</sup>speed of light:  $c = 299\,792\,458$  m/s Bureau International des Poids et Mesures (2006)

## 2.2 Range Imaging Cameras for Testing

At the IPF the ToF camera SwissRanger 3000 (MESA Imaging, Switzerland) was available. The camera is an almost cubic single body instrument. The research group “*Engineering Geodesy*” of the “*Institute of Geodesy and Geophysics*” owns the CamCube 2.0 (PMDtech, Germany). This camera is made up of three cuboid parts. Both cameras are depicted in Figure 2.2. More details about these cameras are given in the following part and in other chapters.

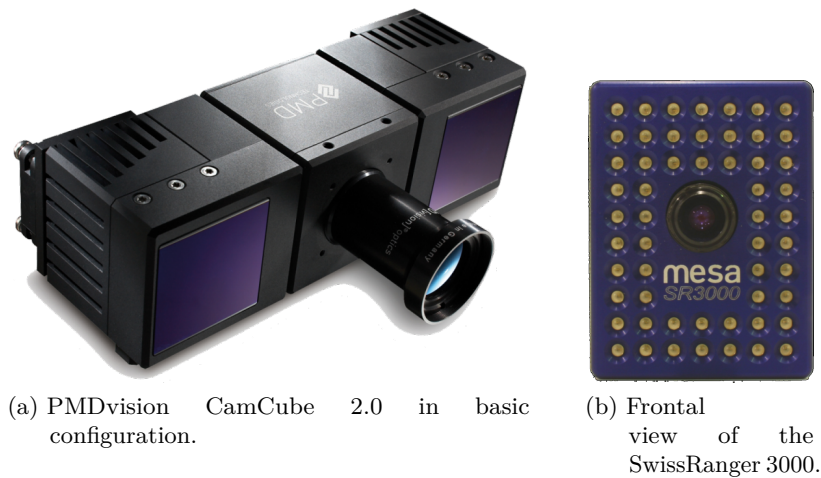


Figure 2.2: The two range cameras used for the experiments.

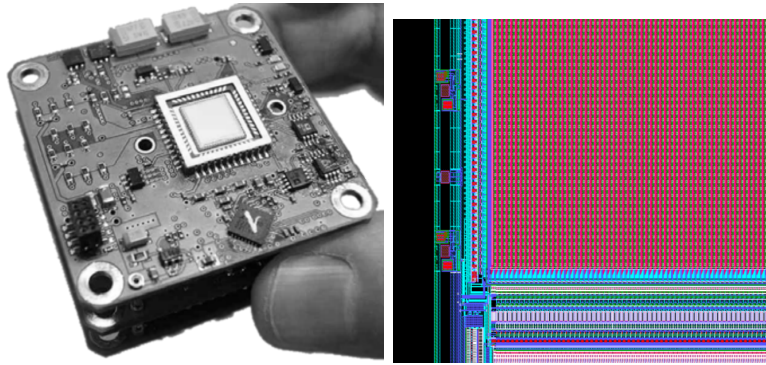
### 2.2.1 The Image Sensors

In general all imaging sensors are subject to thermal diffusion of charges. Aside from optically generated charges thermally generated charges play a dominant role. To keep this effect low the sensor can be cooled down to low temperatures.

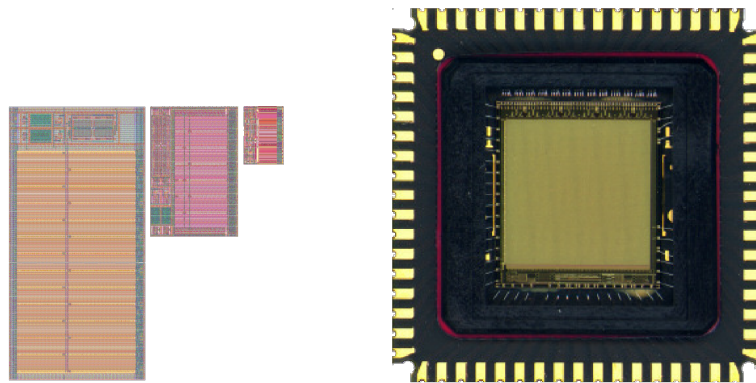
To prevent background light from reaching the sensor an optical band-pass filter is introduced in the SR3000 (Kahlmann, 2007). The CamCube has got filters in front of its illumination units to make sure that unwanted light is not sent out to the object space (see Figure 2.2a).

A so called one-tap pixel samples the signal four times to reconstruct the phase difference (Mesa Imaging, 2006) the two-tap pixel is capable of evaluating twice as much sampling points. This is done by sampling the signal at points with a phase difference of  $\pi$  at the same time. The SR3000 makes use of one-tap pixels while the sensor of the CamCube

uses two-tap pixels combined with averaging of the data. The distance and amplitude is derived from the sampling results in every single pixel.



(a) *left*: Image sensor of the SR3000 with a pixel pitch of  $40\mu\text{m}$  (Oggier et al., 2005). *right*: Detail of the sensor structure (Oggier, 2008).



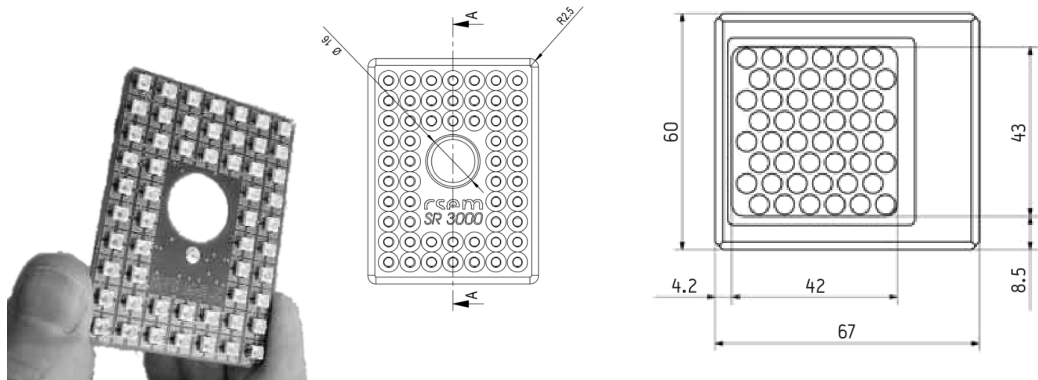
(b) *left*: PMDtech: different chip sizes with pixels of  $210\times 155$ ,  $100\times 100$  and  $45\times 45\mu\text{m}$  (from l.t.r.). *right*: The “PhotonIC’s 41k-S” ( $45\times 45\mu\text{m}$ ) sensor used in the CamCube 2.0 (Frey, 2008)

Figure 2.3: Image sensors of the range cameras.

The cameras ability to suppress background illumination is not only limited to uncorrelated signals, but also to thermically induced charges. This makes the sensor itself usable under difficult temperature conditions (Ringbeck and Hagebeuker, 2007).

### 2.2.2 The Illumination

Figure 2.4 shows both illumination units of the cameras. While the SR3000 has its LEDs around the lens, the CamCube uses two separate illumination units mounted to each side of the main camera body in the basic configuration.



(a) SR3000 IR diodes. (l.: Oggier et al. (2005), r.: Mesa Imaging (2006)) (b) CamCube IR LEDs. (PMD Technologies, 2009)

Figure 2.4: SR3000 and CamCube arrangement of LEDs. (drawings are at the same scale)

Both Cameras use infra-red light to actively illuminate the scene. This is done by using burst modulation. Burst modulation means that several short pulses are sent out rather than a continuous signal. This kind of modulation is mentioned regularly in context of range cameras and is supposed to keep the temperatures low which increase because of the relatively high energetic output of the LEDs. Furthermore, this operating mode reduces the influence of other light sources by consisting of short high energetic light pulses which are in relation to the background illumination much larger compared to continuous illumination (signal-to-background-light ratio) (Oberhauser, 2006) (see Figure 2.5).

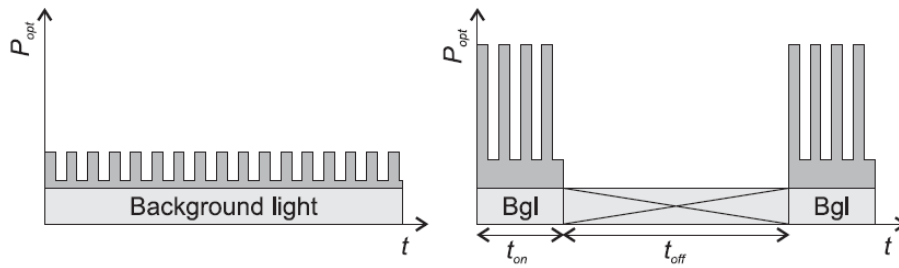
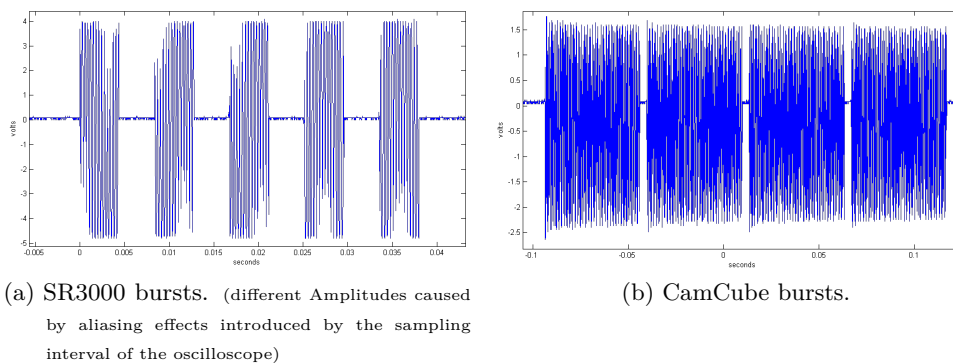


Figure 2.5: Principle of burst-mode illumination (Oberhauser, 2006). Compared to the background light the burst modulation depicted right has a larger ratio of the signal. Between two bursts the LEDs have time to cool down a bit which helps to keep the temperatures low.

Figure 2.6 shows bursts of both cameras. For some reason the SR3000 releases groups of five bursts although the reconstruction of the wave can be accomplished by sampling four times only.



(a) SR3000 bursts. (different Amplitudes caused by aliasing effects introduced by the sampling interval of the oscilloscope)

(b) CamCube bursts.

Figure 2.6: Comparison of bursts of SR3000 and CamCube.

## SR3000

The illumination is realised by an array of 55 IR diodes with a peak wavelength of 850 nm (Mesa Imaging, 2006). They are arranged around the lens (see Fig. 2.4a on the preceding page) to reduce shadowing effects and to have the centre of illumination and the optical centre well aligned. In Kahlmann (2007) it is assumed that the high number of LEDs is chosen because it leads to a nearly sinusoidal signal by averaging out inhomogeneities a single LED could have. A homodyne mixing/detection is used, which means that only a single modulation frequency source is used for the range determination (Lange, 2000).

An IR-detector was built (see A.1.3) for looking at the modulation frequency. Well defined gaps between the emitting periods could be seen which could be traced back to the timing mode of the camera which is responsible for steering the successively integration of the sampling points of the signal (see Figure 2.7 below).

The illumination is switched off when the internal temperature is rising to 46.8 °C. This prevents the Camera from being used in environments up to the specified temperature of 50 °C (see 2.1 on page 13). When cooling down to room temperature the illumination starts again when the sensor temperature falls just below 35 °C. At this temperature the cooling fan stops working on its highest speed and continues with fewer revolutions per minute.

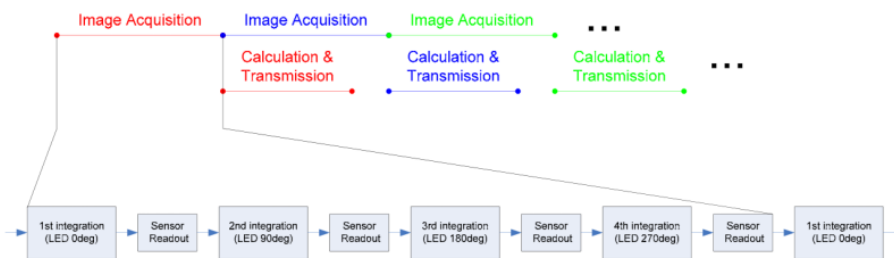


Figure 2.7: Timing schedule of the SR3000 (Mesa Imaging, 2006) showing the repeating cycle of integration and readout phases. The optical dead time between two illumination phases is used to carry out calculations or other processing steps (Lange, 2000).

## CamCube

The CamCube offers connections to two separate illumination units that are mounted to both sides of the camera body and cooled down by a small ventilator each. Those fans are constantly working regardless of the recording state of the camera. Each unit consists of 48 LEDs. In contrast to the SR3000, a filter is placed right in front of the LEDs which is likely there to help to reduce unwanted frequencies of light to be present.

Figure 2.8 shows a typical beginning of a burst sent out by the CamCube's illumination. It can be seen that the first amplitudes are higher than the following ones until a certain level is reached which then remains almost constant besides from small variations. It is not known when the signal is sampled and therefore it cannot be said if the change in amplitude has an effect on the measurement.

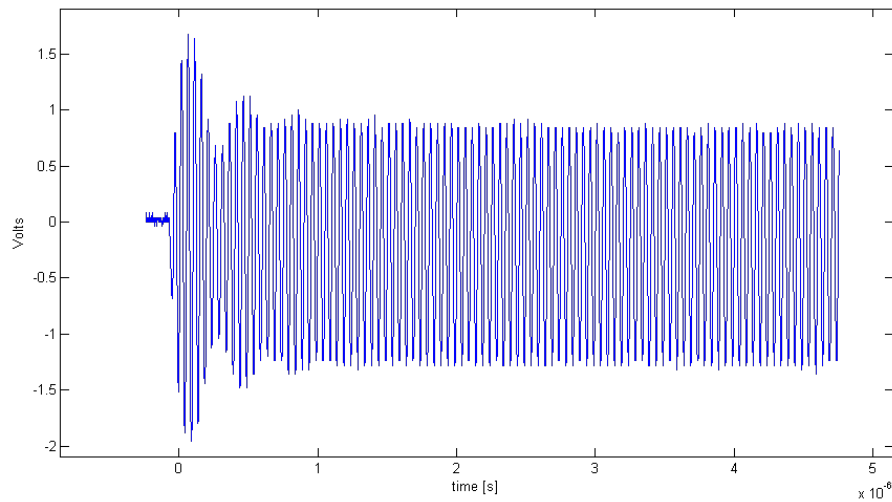


Figure 2.8: Detail of the first moments of a burst (CamCube).

### 2.2.3 The Cooling System

#### SR3000

Aside from the fact that the camera is temperature calibrated (mentioned in Oggier et al. (2005)) nothing is known about how this is done in detail.

The camera itself is cooled by a single ventilator that is driven at different speed levels according to temperature. Air is blown through numerous vents on top and bottom of the housing. To allow proper cooling, the vents need to be kept free during all times. For this reason the camera was mounted as depicted in figure 2.9b (see chapter 3.2 “*Camera mounting*”).



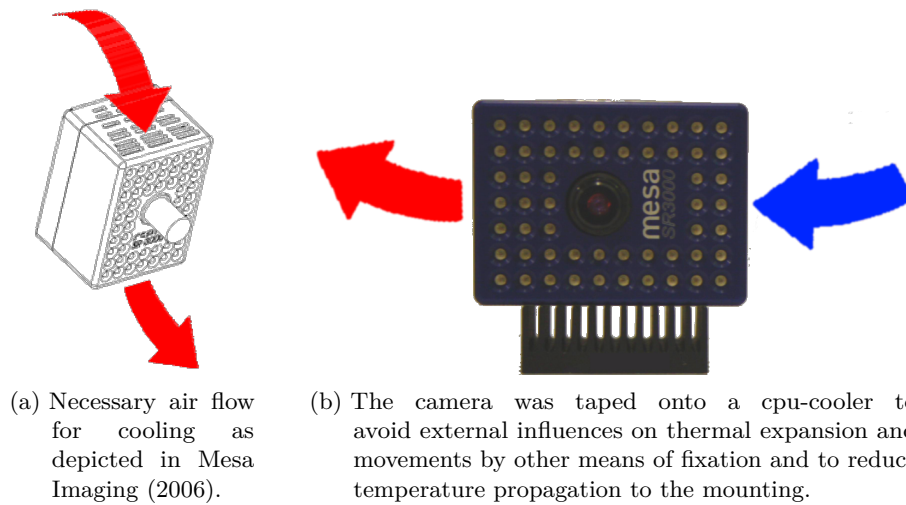


Figure 2.9: Recommended air flow and how it was assured during the experiments.

To find out the levels at which the ventilator started working the camera was started at room temperature via the software from the IPF. The integration time was set to  $4 \times 51.2 \text{ ms}$  because at lower integration times the active cooling did not start. The sensor temperature (see 3.2.1) at which the ventilator started working was found to be  $34.8^\circ\text{C}$  reaching its maximal revolution rate at around  $35^\circ\text{C}$ . The active cooling stopped after the temperature of the sensor fell below  $34^\circ\text{C}$ .

### CamCube

Because the CamCube is based on a modular system without a single body casing the cooling is done differently here. Each illumination unit has got its own cooling part consisting of a passive cooler in combination with a ventilator (see Figure 2.10). The main camera part does not have any cooling vents and is therefore not circulated by air.



Figure 2.10: The active cooling of the CamCube is limited to the illumination units.

## 2.2.4 Overview of Features of the Cameras

Both cameras are specified to quite large temperature ranges which are given in Table 2.1 below. For the experiments it was necessary to heat up or cool down the cameras to the specified temperatures. Therefore instruments described in chapter A.1.1 were used.

	storage	operation	sensor dimensions
CamCube 2.0	-20 °C to +85 °C	0 °C to +50 °C	204*204 [pixel]
SR3000	-10 °C to +75 °C	0 °C to +50 °C	176*144 [pixel]

Table 2.1: Overview of storage- and operating-temperatures. (Mesa Imaging, 2006; PMD Technologies, 2009)

Later in 2011 another fact-sheet of the Swiss Ranger was found (Mesa Imaging, 2008) with differing temperature ranges for operation (-10 °C to +50 °C). This could not be taken into account, as most experiments would have had to be retaken and other means for cooling would have had to be organised.

Table 2.2 states some values of the optical system and illumination system.

	focal length	modulation frequencies
CamCube 2.0	12.8 mm	18, 19, 20, 21 MHz
SR3000	8.0 mm	20 MHz

Table 2.2: Focal lengths and often used modulation frequencies of the cameras. The modulation frequencies can be varied. (Mesa Imaging, 2006; PMD Technologies, 2009)

## 3 Considerations on Setup

All of the findings of the following subsections led to the final experimentation setup. The cameras were put on top of a metal plate supported by a surveying tripod. A flat target with printed circles on it was about one meter away.

### 3.1 Geometry of the Object Space

#### 3.1.1 Geometry of the Target

Because of the nature of the experiments and the focus only on the influences of temperature and temperature-changes a special object space was not necessary. To avoid effects of multiple reflections a corner formed by two walls is not a suitable choice.

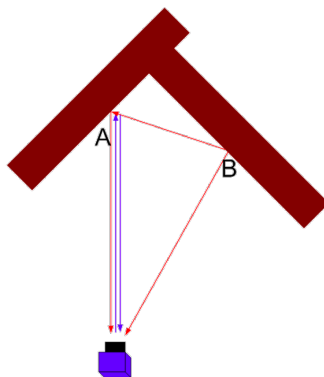


Figure 3.1: Multipath effect caused by reflections from the adjacent wall. The direct measurement to the wall in front of the camera (Path A) is influenced by reflected light (Path B) (Mesa Imaging, 2006).

A plain white surface with a printed pattern on it was chosen as target plane. This should ensure a sufficient contrast of the received amplitudes for a precise target determination. The pattern itself should be large enough to be usable with both RIMs. A pattern of black circles with a diameter of three centimetres and a grid size of 15 cm was printed on

standard plotter paper. As stated in several publications standard office paper has very homogenous reflecting properties.

### 3.1.2 Target Distance

The basic idea of the setup is to keep things as simple as possible in order to concentrate on temperature effects only. This leads to an arrangement that is close to the photogrammetric normal case. This way effects of different angles of incidence by the illumination are mostly avoided.

The distance was kept relatively short with around one meter. This way the signal to noise ratio should be high enough and not unnecessarily decreased by a too large distance and then smaller amplitude. The influence of temperature should be seen regardless of the distance itself.

The distance to the target was chosen to be close enough to provide almost noise free data and according to the grid of black dots described in chapter 3.1.1 above. Because both cameras have similar angles of view of roughly around  $40^\circ$  in both dimensions the same position of the tripod could be used. The position was chosen in a way that the target circles were present well in the corners of the derived images. Figure 3.2 shows examples of the target distribution within a frame. The accuracies of the derived centres of the target corresponded to the amplitude very well as expected.

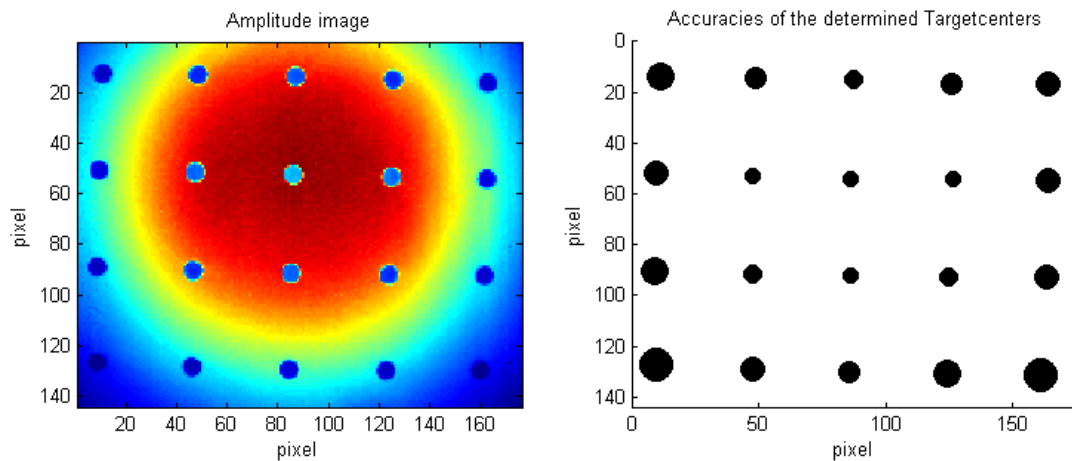


Figure 3.2: *left*: Typical amplitude image derived by the SR3000. A vignetting effect can be seen related to the illumination intensity. (red = high, blue = low)  
*right*: Accuracies corresponding quite well to the amplitudes. (small = good)

## 3.2 Camera mounting

Both cameras have standard photographic 1/4" threads. The SR3000 has its thread on the back while the CamCube's thread is on the bottom in the middle.

For the experiments it is necessary to put the instruments repeatedly into the same place in order for the results to be comparable. Also the repeatability of experiments should be assured this way.

Due to the size of the quick-change plate of the first tripod used, it was not possible to plug in the USB connection of the SR3000. As workaround a bent threaded rod mounted onto a quick-change plate was used. As this fixation method might had too much influence by its 12 cm long threaded rod that was warmed up together with the camera and therefore subject to thermal expansion.

The CamCube is also compatible with standard quick change plates which allow a quick and uncomplicated placement of the camera to guarantee only marginal temperature changes between setting up and starting the measurements. Nevertheless, the same tripod with the metal plate on top was chosen in order to guarantee the same stability performance of the tripod for both cameras. The order of switching on before setting up was adopted later to account for switch on effects.

The supporting construction can be seen in Figure 3.3. It consists of an aluminium plate with a hole matching the thread of the connection piece to the tribrach. Each side of this plate was prepared for another camera.

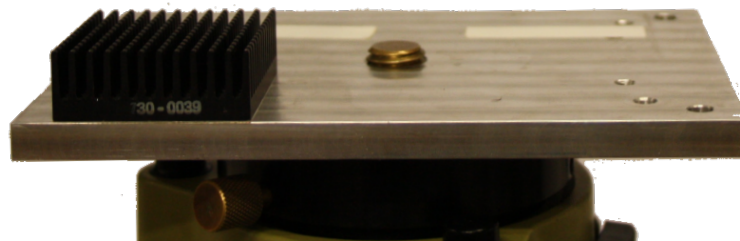


Figure 3.3: Metal top of the tripod with places for the CamCube and SR3000.

The SR3000 was supported by a passive CPU cooler that was mounted on one side to avoid contact with the entire side of the housing and make sure that there was as little influence of the mounting on the heat transfer as possible. The other side was prepared for the CamCube with only two strips of double-sided tape below the illumination units to hold the camera in place. This was done for security reasons because the camera's weight should be enough to prevent itself from moving around while lying there. Due to the massive construction of the instrument, it was assumed that special precautions concerning the heat transfer, as for the SR3000, were not necessary.

The depth of the metal plate was enough to support the various cable connections to the cameras so that no disturbing pulling force was able to come from there.

### 3.2.1 Temperature Tapping

A magnetic temperature probe (details in chapter A.1.2) was intended to monitor the housing temperature of the cameras. Because the housing of the SR3000 is made of aluminium it is not magnetic. Also the CamCube has a lack of reachable magnetic parts that can be considered representative for the housing temperature. To solve this problem, little steel sheets were taped to the surface using a heat transfer compound to ensure good contact and fairly accurate temperature measurements. Other advantages were the quick mounting procedure of the thermal sensor without the use of fixing materials and the perfectly repeatable sensor position. Figure 3.4 shows the CamCube with two different positions of heat transferring metal sheets and the SR3000 with one on its side.

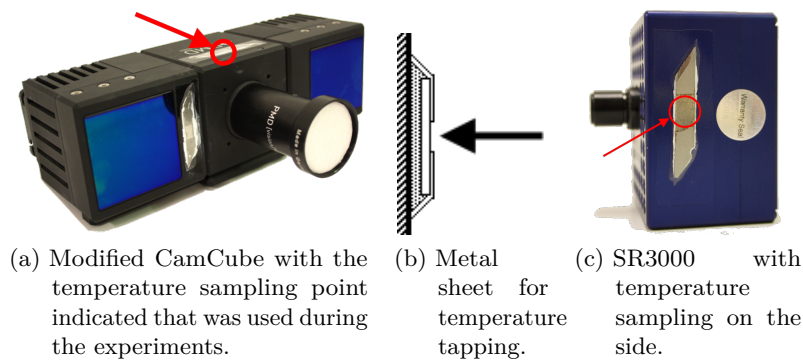


Figure 3.4: The range cameras with additional sheets of metal for better heat transfer.

Additional the temperature right next to the imaging sensor of the SR3000 could be read out with the IPF-software. This temperature was seen as identical with the temperature of the sensor itself. It was not possible to read out an internal temperature of the CamCube and maybe such an internal sensor does not even exist.

### 3.2.2 Camera Support

To make sure that the tripod was steady enough an experiment was carried out using the SR3000 at room temperature. The aim of this experiment was to see if the position of the target points was constant or not. During a period of five hours the target pattern was

recorded at almost constant instrument temperature. The result is shown in Figure 3.5 and shows only minimal random movement of the projection of the target on the chip.

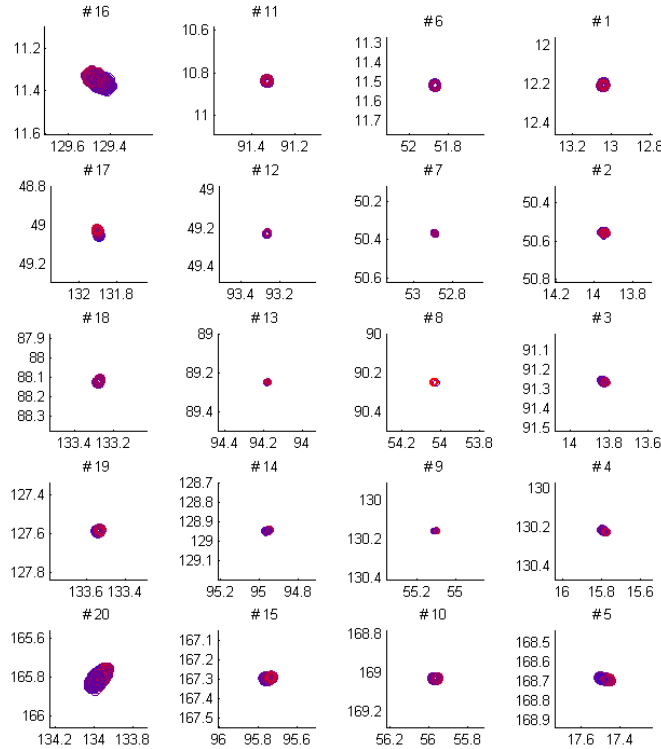


Figure 3.5: Check of steadiness of the Support carried out with the SR3000. The recorded Targets only show marginal movements without a certain trend.

Figure 3.6 shows the four targets in the corners. The rotated camera is already taken into account as can be seen by the numbering of the targets. Three of those targets show almost circular distributions of the determined target centers with random deviations in horizontal and vertical direction. Only target number 5 shows another pattern. This behaviour could not be interpreted.

The mean of all coordinate ranges of all targets was found to be 0.08 pixels and without target number 20, which was an outlier in this matter, the figure was even lower with just below 0.04. When not using the targets in the corners which suffer from worse illumination conditions this value can be reduced to 0.03. The vertical range was found to be smaller than the horizontal range which confirmed the steadiness of the support.

Compared with usually obtained ranges (up to 0.2 px) of target positions during experiments with temperature changes this is by far good enough.

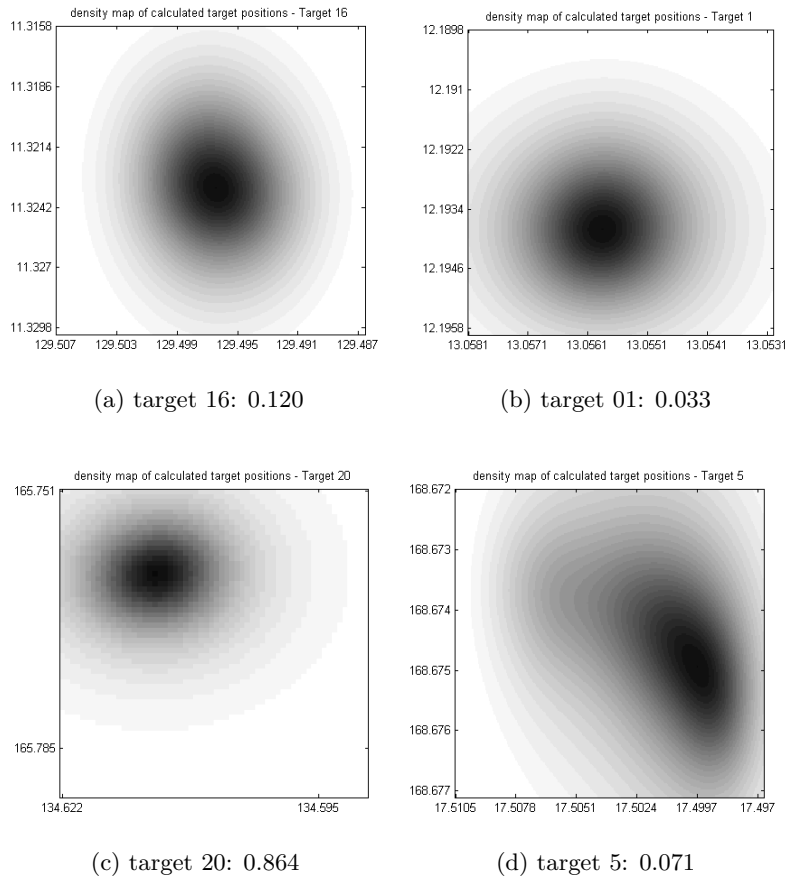


Figure 3.6: Targets recorded by the SR3000 during a 5 h long experiment. Corner targets and their maximal coordinate range in pixels. Due to the low accuracy in the corners those values represent upper limits.

### 3.3 Ambient Light

The influence of ambient light was investigated in a section in Pattinson (2010) and seen as negligible. Furthermore it was shown that detected frequencies that are even harmonics of the modulation frequency do not have any influence on the distance measurement because of how the integration on the chip is done (Lange, 2000), possibly reducing the impact of light sources which run on usual electrical outlets.

In the surveying laboratory that was used in this work fluorescent tubes are used for illumination as was the case in Pattinson (2010). Also actual research by SAJID GHUFFAR



and WILFRIED KAREL did not entail any differences between measurements with lights either turned on or off. Therefore it was no longer paid attention to the lighting situation but nevertheless kept constant during the experiments.

### 3.4 Ambient Temperature

To see if a temperature variability in the measurement laboratory was present, a thermometer was used to log this parameter.

The temperature variation of the test environment was monitored over a longer period of time using a digital thermometer. Data collected from 22.12.2010 until 18.2.2011 only show a total variation of about 4 °C, which is depicted in Figure 3.7. This variation was reduced after the ventilation of the laboratory was turned on later during the year.

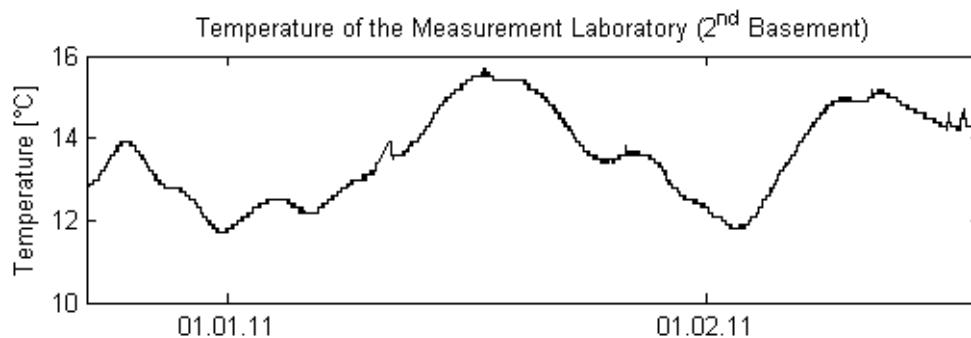


Figure 3.7: The temperature of the Laboratory two month from 22.12.2010 on.

In general it can be said that only small temperature variations occur in the measurement laboratory. Due to stable temperature conditions under which the experiments were conducted, permanent monitoring of the ambient temperature at a high rate was not required.



Figure 3.8: The final set up. Tripod with mounting plate on top around one meter away from the target pattern on the blackboard.

A detailed overview of the effects of the external temperature on the measurements of the SR3000 is given in Kahlmann (2007). Due to the lack of proper climatic instruments such specialised experiments could not be carried out.

Nevertheless, in contrast to systems with the demodulation process taking place in separate electronic components the on-chip demodulation process' advantage is that other temperature-critical or ageing electronic parts are not present or at least very few of them (Lange, 2000).

## 4 Methods

### 4.1 Data Acquisition

Depending on the camera used, the operating system with the relevant recording software was used. While the datafile from the SR3000 could be directly read frame by frame with MATLAB, the \*.bin-file from the CamCube had to be converted and was split into single \*.m files. After extracting and merging the data from the external thermometer, the data structure had the same format and could be easily used with only one ongoing evaluation algorithm. Figure 4.1 shows the data transition from recording to the calculations. The raw frames have 16 bit and values are therefore scaled between 0 and  $2^{16} = 65\,536$ . If not stated otherwise amplitudes are represented by those raw values.

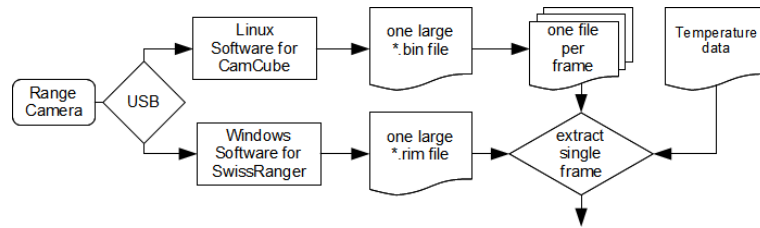


Figure 4.1: Data recording with both cameras and harmonisation.

Because of the huge data quantities either a fast external storage or the use of only one OS on the recording computer is recommended for future recordings. Another solution would be to change the recording in a way that only necessary information is taken (e.g. only distance images).

### 4.2 Experiments

In Weyer et al. (2008) a minimal warm up time of six minutes is recommended based on their experiment. In Steiger, Felder, and Weiss (2008) stabilisation was reached after at most 250 s (=4 m 10 s). For the experiments carried out in this work the measurements started around six minutes prior to the placement of the cameras at room temperature.

Because of separate ways of heating or cooling the cameras two runs were necessary most of the time. Results were merged into a large dataset covering the whole temperature range according to Figure 4.2.

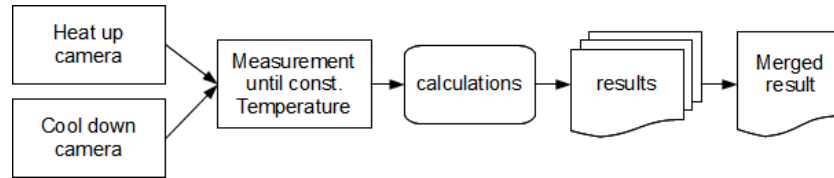


Figure 4.2: Merging of data from experiments.

### 4.2.1 Determination of the Target positions

The determination of the target positions was done using MATLAB as depicted in Figure 4.3. For the determination of the centres the amplitude images were used. The use of the distance-image was not possible due to the fact that a flat target pattern was in use.

First of all the image was segmented according to the type of camera because a determination of the targets all over the image could not easily be carried out due to the wide range of amplitudes making a single threshold impossible. Because of different fields of view the CamCube had 5x5 targets in view while the SR3000 “saw” 5x4. The value of the variable “rimType” was used as switch in the calculations and assured a homogeneous data-flow.

The same target distance was used throughout the experiments. Therefore the same amount of targets was in the field of view every time depending on the instrument used.

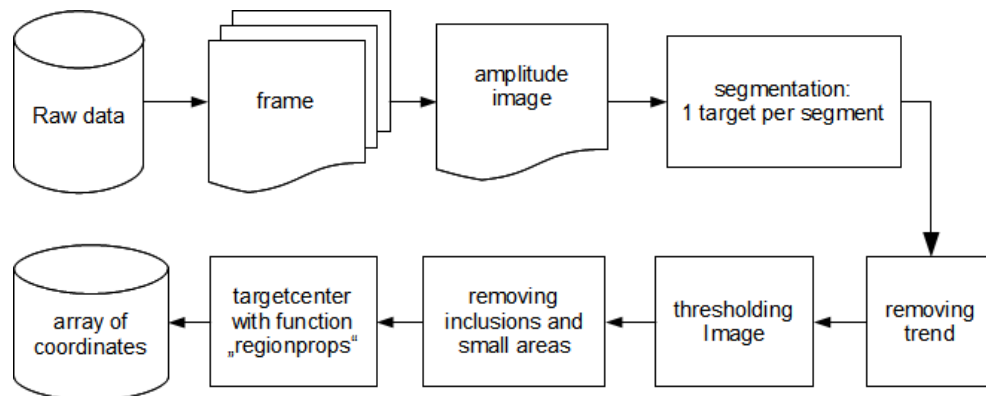


Figure 4.3: Getting rough target positions in MATLAB.

The derived rough target positions were used as an input parameter for more precise target calculations. Therefore a square area around the estimated position was used as input parameter for the function *fitCumGauss* that was available at the IPF. This function uses a cumulated gaussian distribution as reference figure to describe circular targets. This function uses a black image containing a white target. As the standard scaling delivers the inverse grey scale the negative had to be used. More details are described in chapter “4.2.2. 2D Gaussian Distribution Fitting” in Otepka (2004). The fitted target center as well as the accuracy of the center were used for the evaluation.

#### 4.2.2 Differences in Dark Current distribution

The distribution of the dark current was investigated by calculating an average plane through each amplitude image (see Fig. 4.4). A change due to temperature was expected and found in data from the CamCube. Details are given in 5.3.1 on page 36.

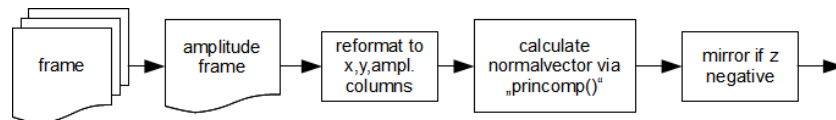


Figure 4.4: Calculation of the normal vector of an amplitude image.

# 5 Results

## 5.1 Influence on Measured Data

The target described in chapter 3.1.1 was used throughout the experiments. Most scatterplots in this chapter are based on the temperature and not on time and are colour-coded to ease the interpretation.

### 5.1.1 Permanence at Room Temperature

#### SR3000

A long time experiment carried out by WILFRIED KAREL was used to additionally monitor the temperature of the instrument itself. In this experiment the SR3000 was used to record a black surface for a period of several hours.

The temperature of the housing was found to be constant aside from variations in the order of the thermometer's accuracy. The internal temperature (next to the sensor see 3.2.1) varied at most  $0.74\text{ }^{\circ}\text{C}$  but mainly only by  $0.49\text{ }^{\circ}\text{C}$ . Other long term experiments showed similar results.

Looking at the sensor temperature of the 5 h-experiment used already in chapter 3.2.2 revealed a periodic change of the internal temperature of around  $1\text{ }^{\circ}\text{C}$  at a frequency of about 25 s. Distances and amplitudes were found to change at the same rate which is consistent with the findings of Karel, Ghuffar, and Pfeifer (2010).

#### CamCube

Because of limited storage space for the recorded data a long time experiment of comparable duration like above was not possible. Instead a closer look at the temperature of the camera was taken.

The CamCube was left in standby for around an hour resulting in a relatively high but stable temperature. It is not clear why the camera was getting hotter without carrying out measurements. The temperature of the housing was taken with a surface probe (thermo-electra 80102A, see Chapter A.1.2 on page 54) to get an idea of the temperatures of the different parts of the camera. Table 5.1 summarises the measured peak values, while a more intuitive image of the distribution can be seen in Figure 5.1.

---

part of the camera	min.	max.
overall	23.7	27.7
Camera	26.7	27.7
Illumination	23.7	25.8

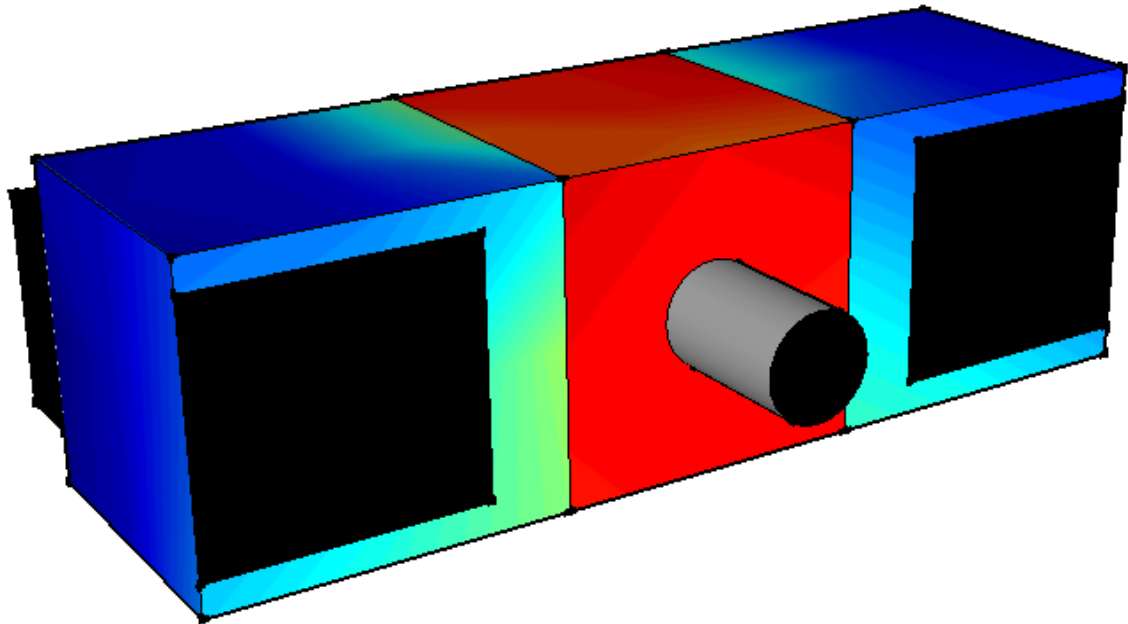
Table 5.1: Maximal and minimal temperatures measured at the CamCube while on standby in [°C].

It was noticed that both illumination units had quite similar or rather almost identical heat distributions. The passive cooling elements ventilated by a fan were rather cool, while only the more massive parts and areas with poor air flow heated up to around 25.7°C.

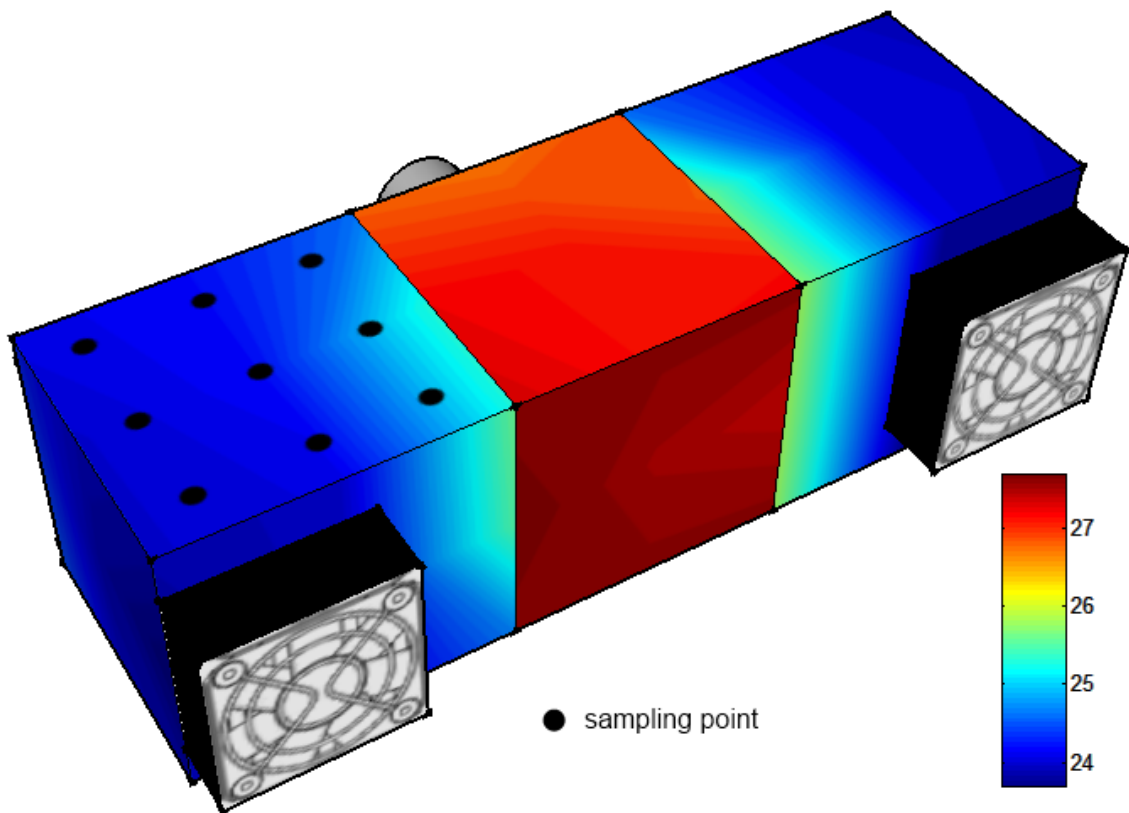
The camera itself did not heat up uniformly but up on one side more than on the other. This might be an effect caused by the fact that on the warmer side the electrical power enters the instrument. A more detailed investigation if this temperature gradient was related to the specific dark current distribution can be found in chapter 5.3.1.

Because of a small gap to the central camera cube the heat transfer amongst the different parts was limited as Figure 5.1 suggests.

every accessible face of each cube was sampled at nine points as indicated below



(a) Front view of the CamCube.



(b) Back view of the CamCube.

27

Figure 5.1: Qualitative temperature distribution of the CamCube in standby after reaching a steady state.



### 5.1.2 Influence on Distance

#### SR3000

As described before, two different temperature sampling places were available. Namely the temperature of the sensor itself and the temperature of the housing. Several effects were observed when looking at the distances. The results depicted in Figure 5.4 were derived from data collected at two consecutive days and merged as described in Chapter 4.2 on page 22. The difference in the distance of around one centimetre between both constant states (the two clusters where the experiments meet in the Figure below) of the experiments can not be explained definitely.

Looking at the diagram about the relation between the sensor temperature and the distance in Figure 5.2 gives a hint of a hysteresis that might occur if the whole cycle is carried out at once. A linear fit of the warm-up phase gives  $1.4 \text{ mm}/^\circ\text{C}$  while the fit of the cooling-down part gives around  $2.1 \text{ mm}/^\circ\text{C}$ .

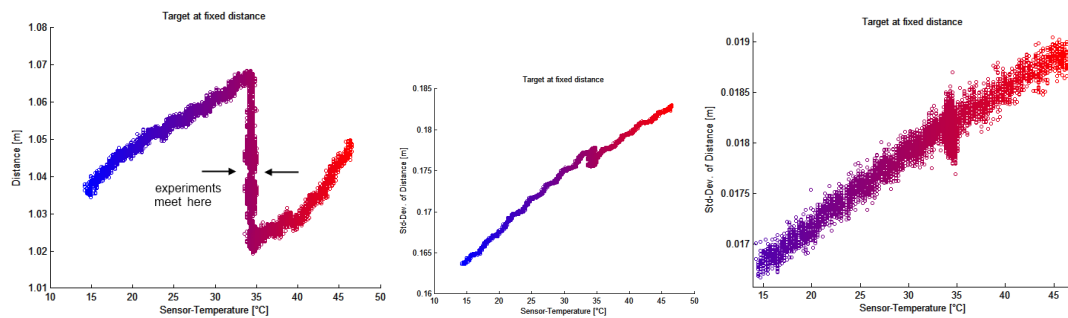


Figure 5.2: left: Sensortemperature versus distance. middle: sensortemperature versus standard deviation of the distance of a single frame. right: same as middle but with the mean of 10 frames as reference.

The relation between the temperature of the sensor and the standard deviation of a single distance-frame image gave a gradient of  $0.72 \text{ mm}/^\circ\text{C}$  in the cold part (without ventilation) and  $0.52 \text{ mm}/^\circ\text{C}$  in the warm part (with ventilation).

Using 10 frames as reference, the standard deviation of the difference of the actual and the reference frame showed a linear dependence from 16.8 to 18.9 mm aside from outliers that were mostly present around the already mentioned range of unsteady operation of the ventilation. A robust linear fit resulted in gradients of  $0.038 \text{ mm}/^\circ\text{C}$  (cold) and  $0.027 \text{ mm}/^\circ\text{C}$  (warm).

Using the housing temperature that was taken simultaneously resulted in not as clear connections to the measured data because of the lag in temperature as can be seen in

Figure 5.3. Those results were not further investigated but show the difference that could be introduced by using housing temperatures only. The differences are explained more exactly later in this chapter.

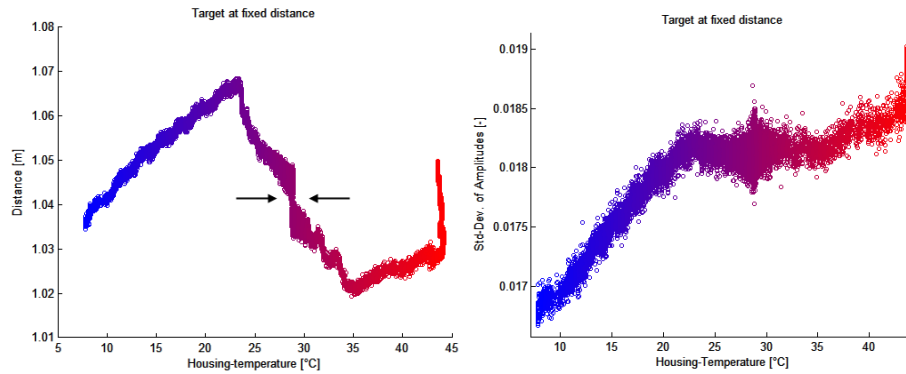


Figure 5.3: Housingtemperature versus distance and housingtemperature versus the standard deviation of the distance.

Looking at Figure 3.42 on page 84 of Kahlmann (2007)<sup>1</sup>, some basic similarities might be interpreted but those are too vague to be mentioned here. Because of the closed temperature cycle used in that publication some differences between the warming and cooling can be detected as expected. However this was not the main focus although it might be of interest for further investigations.

<sup>1</sup>only external temperatures are used in that work

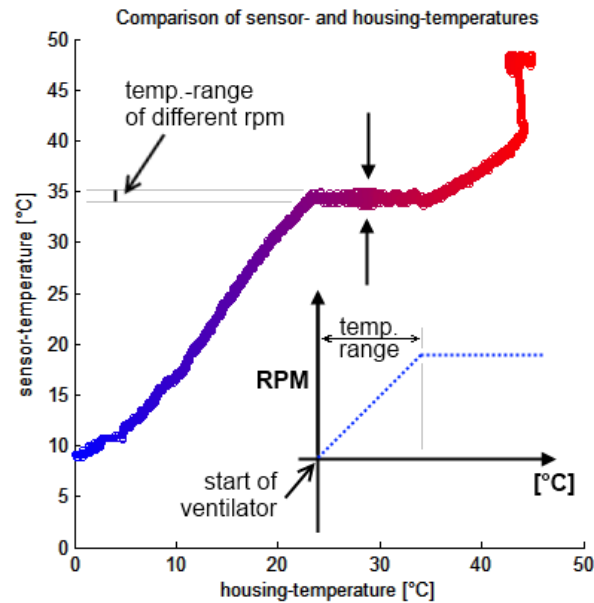


Figure 5.4: Housingtemperature of the SR3000 compared to the sensors' temperature. The temperature is rising slower when the ventilator is working.

Figure 5.4 shows that the sensor temperature remains constant from the start of the ventilator onwards, (see chapter 2.2.3) while the housing keeps heating up. Both temperatures start to rise again when the ventilator reaches its maximal r.p.m.

### CamCube

As already explained in Chapter 3.2.1, only housing temperatures were available during the experiments done with the CamCube.

It was seen that during the warming up process condensed water occurred on the filters in front of the LEDs as also described in other publications. The influence can be seen in Figure 5.5. It is therefore not recommended to use the camera during this period or take the different behaviour of the camera into account. Using only data from the part of the experiment without water, a gradient of around  $4 \text{ mm}/^\circ\text{C}$  was found for temperatures below room temperature. As the dependence is not quite linear above room temperature, a more advanced model is needed. It was found that a polynomial model of order six fits the whole temperature range quite good. Otherwise a more or less linear dependence of roughly  $4.4 \text{ mm}$  can be approximated in the range below  $40^\circ\text{C}$ . The almost vertical part around  $54^\circ\text{C}$  (left in Figure 5.5) lies not within the specified working temperature range.

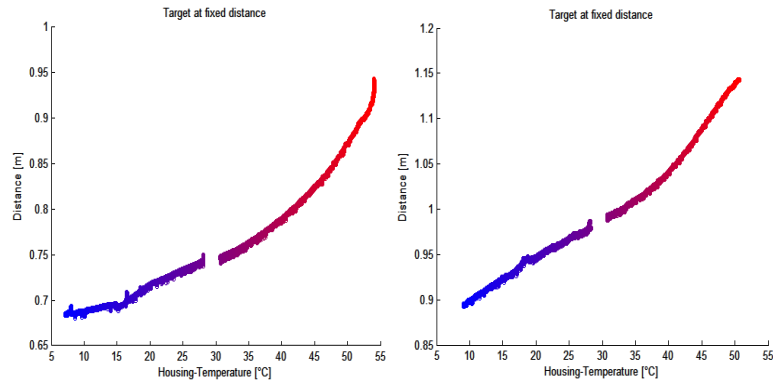


Figure 5.5: Dependence of distance on temperature. The second experiment right was started at an higher temperature and is therefore not that much influenced by what is most likely to be condensed water (see below).

A look at the standard deviations depicted in Figure 5.6 reveals interesting things. The influence of condensed water on the instrument can clearly be seen and is likely to be related to the part to the left of the abrupt drop present at around 22 °C. This effect is even more obvious when looking at the amplitude data in the following chapter.

The standard deviation within a single distance-frame (Fig. 5.6 left) shows a quite linear behaviour above the point the condensed water is more than likely to have evaporated. The higher number of outliers in the colder part is not as expected but using the average of 10 frames as reference distance gave another view on this fact. As the right image in 5.6 shows, the outliers are more likely to occur during higher temperatures. The lack of outliers below 22 °C could be traced back to a certain amplitude level.

The linear part between 22 °C and 50 °C has a slope of 2.8 mm/°C.

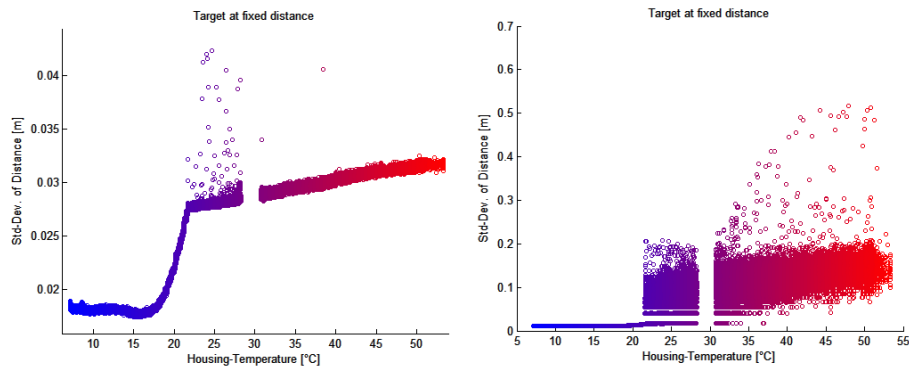


Figure 5.6: Relation between the housingtemperature and the standard deviation of the distance.

### 5.1.3 Influence on Amplitude

#### SR3000

A Look at the amplitudes reveals a large gap between the two parts of the experiment in Figure 5.7. The shift of the gap in temperature is consistent with the shift in the distance experiments described above. Looking at the right picture, clusters at the end of both series at around 35 °C are shown. They occur at around the temperatures the ventilator is switched on and off and delivers different distances (Fig. 5.2).

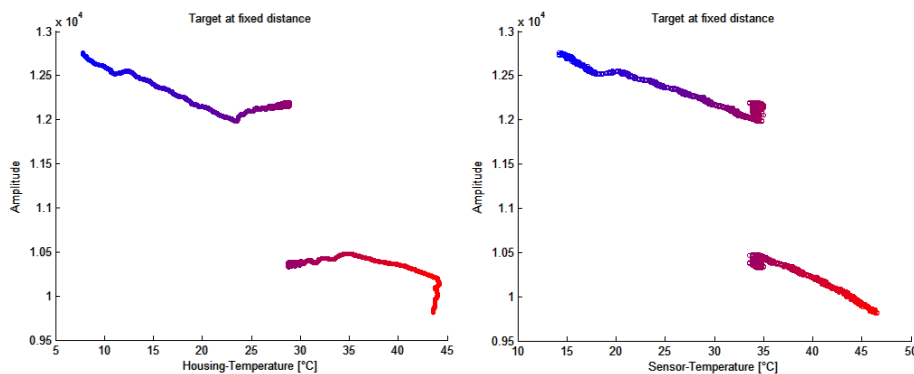


Figure 5.7: Amplitudes recorded during one experiment with the SR3000 related to internal and external temperature sampling points.

A closer look at the repeatability of the amplitude measurement was carried out later in order to find out if this is simply related to two different set ups. A check of the distance

resulted in a mean difference of around 0.8 mm. The comparison of the raw-amplitudes showed only a deviation of -2.5 and for this reason the large gap above can not be explained sufficiently.

### CamCube

While the distance is almost linear during the cooler period (see Fig. 5.5), the amplitude rises sharply after a downfall. Maybe the temperatures of the sensor and housing are not as similar as assumed. Another explanation would be the existence of condensed water. The instruments illumination and lens were cleaned before the selected frames were recorded so that it is possible that after a high starting amplitude water was condensing up to a certain point where it began to vanish again because of the higher temperature. Nevertheless the warm parts seem to have a slope of around -0.18 % which closely accords with the findings of chapter 5.3.4 on page 45.

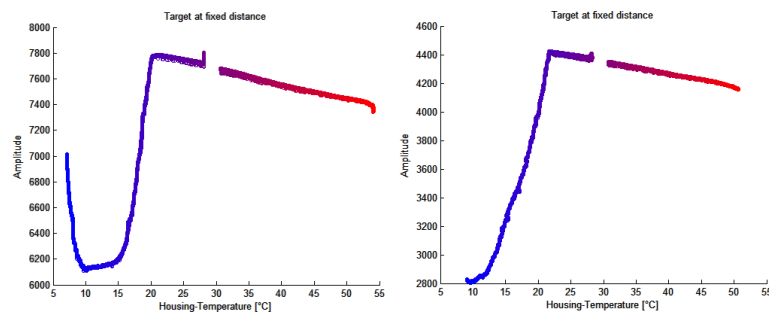


Figure 5.8: The relation between temperature of the housing and raw-amplitudes.

Figure 5.9 shows the standard deviation of an amplitude-frame with 10 following frames averaged as reference. The linear part between 22 °C and 50 °C has a slope of -0.23.

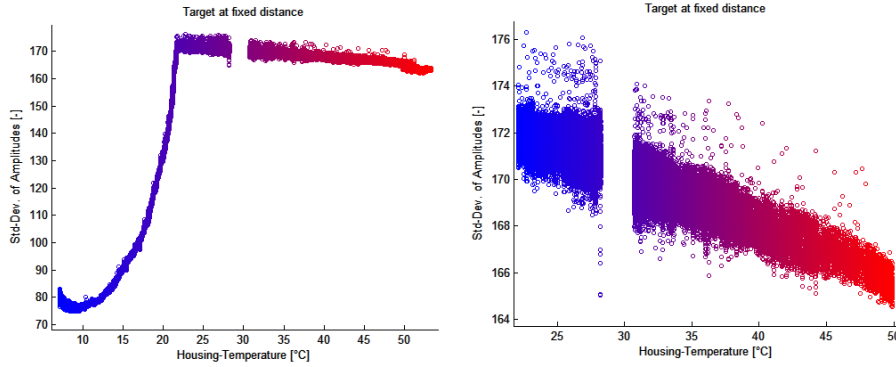


Figure 5.9: Relation between temperature of the housing and the standard deviation of the amplitudes. The right diagram depicts the linear part of the left diagram.

## 5.2 Influence of the integration time on internal temperature

A series of experiments was carried out to evaluate a possible temperature dependence of the internal camera temperature with respect to the chosen integration time. Steps of  $5 \text{ bit}^2$  were chosen in a reasonable range so that no major overexposure of the data was present. Figure 5.10 shows an existing relation. A robust regression results in a linear function of  $0.0022x + 34.29$ .

The correlation coefficient  $r_{xy}$  between integration time and internal temperature was used to calculate the comparison value  $\hat{t}$  which was checked against the security level  $S_{(95\%)}$  to see if this relation was significant (see Formulas 5.1, 5.2 and Table 5.2).

$$r_{xy} = \frac{\sum_{i=1}^n (x_i - \bar{x})(y_i - \bar{y})}{\sqrt{\sum_{i=1}^n (x_i - \bar{x})^2 \cdot \sum_{i=1}^n (y_i - \bar{y})^2}} \quad (5.1)$$

$$\hat{t} = \frac{r_{xy}\sqrt{n-2}}{\sqrt{1-r_{xy}^2}} \quad (5.2)$$

$k$	1	2	3	4	5	6	7	8	9	10	15	20	25
$S_{(95\%)}$	12.71	4.30	3.18	2.78	2.57	2.45	2.365	2.306	2.262	2.228	2.131	2.086	2.060

Table 5.2: Safety limits  $t_s$  for a two-tailed statistical security  $S$  of 95% depending on the redundancy  $k$ .

<sup>2</sup>The integration time is set by changing an 8 bit register of the SR3000. The range from 200  $\mu\text{s}$  to 51.2 ms corresponds to 0 to 255. (Mesa Imaging, 2006)

The present relation turned out to be significant even with the removal of one possible outlier.

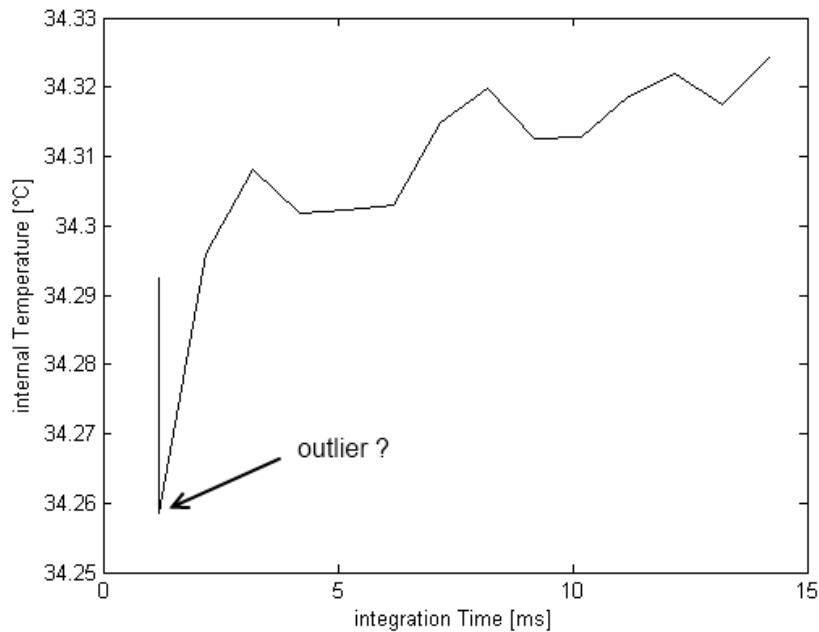


Figure 5.10: Temperature of the sensor related to the chosen integration time.

This result could be subject to closer investigations. A comparison with the distance dependence on integration time found by Weyer et al. (2008) could reveal if the distance relies on the integration time or on the increased temperature as result of longer integration time.

Carrying out this time consuming experiment with the CamCube was considered not purposeful as the exact relation between the housing temperature and internal temperature was unclear and only slight variation was expected.



## 5.3 Influence of Temperature on the Electronics

### 5.3.1 Dark Current in the Sensor

Following chapter “4.2 Noise limitation of range accuracy” in Lange (2000) the range resolution  $\Delta L$  of a four tap demodulation system is:

$$\Delta L = \frac{L}{8} \cdot \frac{\sqrt{B + N_{pseudo}}}{2 \cdot A} \quad (5.3)$$

- $L$ : Non-ambiguity distance
- $A$ : Demodulation amplitude
- $B$ : Acquired optical mean value
- $N_{pseudo}$ : Additional induced electrons

The presence of temperature generates electrons (dark current) that cannot be distinguished from optically created ones. Therefore they are integrated the same way. It was now of interest to see if the dark current was evenly distributed within the sensor or not.

Experiments with covered lens to prevent external light to enter the system were carried out. The illumination was covered to make sure that modulated light could not be detected.

The single steps to the results depicted in Figure 5.11 can be found in Chapter 4.2.2 on page 24. The images show that the distribution of the dark current is not equal throughout the sensor. The x and y-parts of the normal vector were calculated from amplitude images and the corresponding adjusted planes. While the SR3000 shows mostly constant proportions in both directions with only slight changes, the two parts of the CamCube show an obvious change with temperature. The relation of the dark current distribution to the heat distribution within the instrument is researched below.

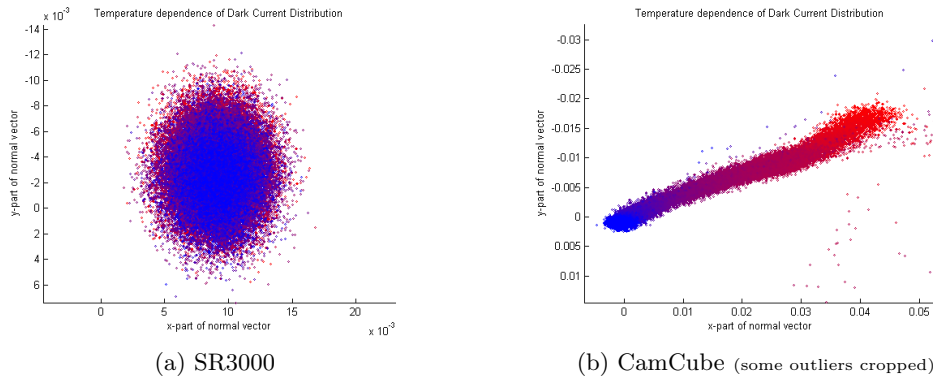


Figure 5.11: Temperature dependent distribution of dark current. Shown by the x- and y-parts of the normal vector of the amplitude frame. (the colour-coded temperature range in both images covers around 0-50 °C)

As expected, the cameras showed smaller signals at lower temperatures which is shown in Figures 5.12 and 5.13. The distribution of the amplitudes did not change along with the temperature. This suggested that the sensor's pixels can not be characterised the same way. This might result from the production process which would make a chip-dependent correction necessary. A hint is given by the structure of the sensor as already depicted in Figure 2.3 on page 7.

The CamCube in contrast did not show such a regular increase over the chip area as the SR3000 did. It can be seen that the amplitudes increase in one corner and spread mostly in the lower left corner. This might be related to different temperatures of the sensor or within the housing but could not be verified. Additionally an effect caused by the way the pixels are read out was thought of.

Subplots are scaled individually. The mean temperatures and amplitudes can be found in the titles of the plots.

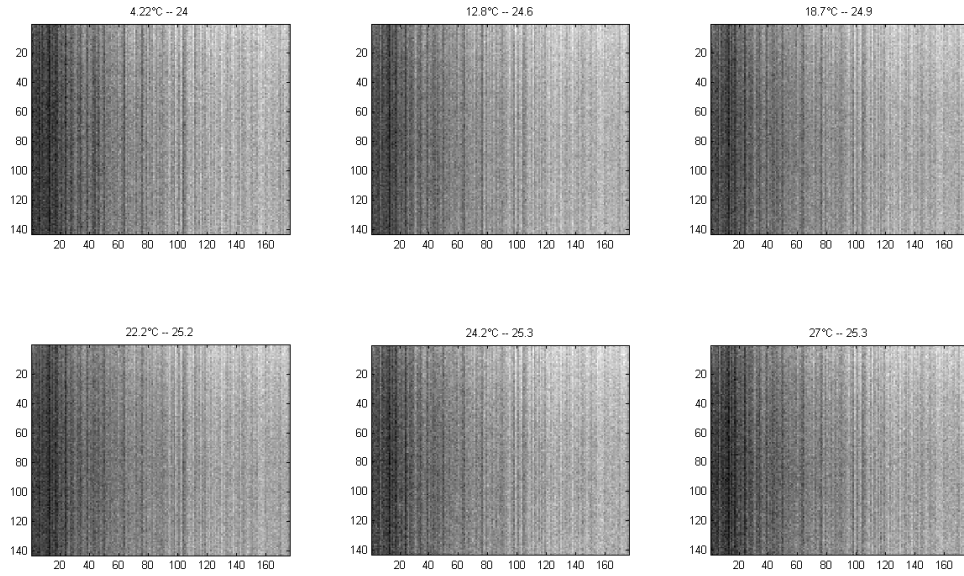


Figure 5.12: Dark current amplitude distribution of the SR3000.

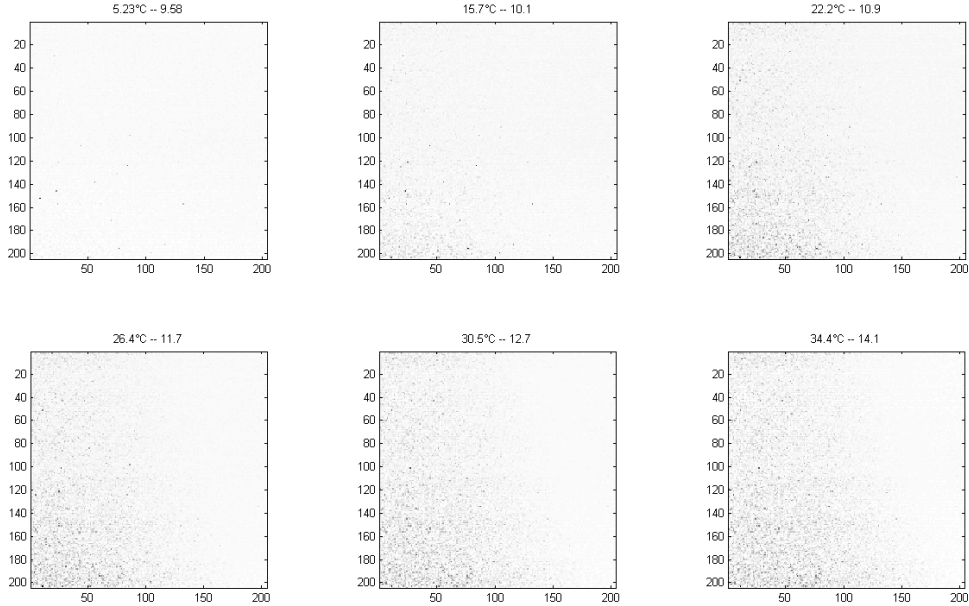


Figure 5.13: Dark current amplitude distribution of the CamCube.

According to Möller et al. (2005) the dark current doubles with every rise of 8 °C. This number is not explained in detail. My results show an quadratic relation in this context.

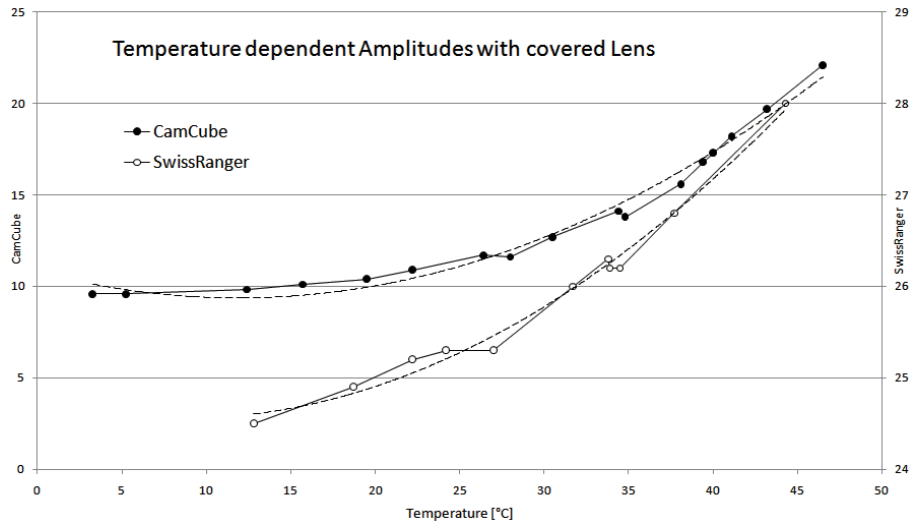


Figure 5.14: Temperature dependence of the dark current amplitudes compared to quadratic functions (dashed).

### 5.3.2 Geometric stability of the imaging sensor

The influence of temperature on the physical dimensions of the image sensor was thought to be not of big influence due to its small sizes. To estimate the expansion of the sensor it was seen as appropriate to follow Trassinellia et al. (2005) chapter 2.4 “Temperature dependence of the pixel distance”.

A thermal expansion coefficient of silicon of around 2.60e-6 is assumed according to Lyon et al. (1977). Furthermore the chip size is assumed to be 40 μm \* 176 px in the larger sensor dimension of the SR3000. Using formula 5.4 with mentioned values only a marginal expansion of 0.9 μm is caused by a temperature change from 0 to 50 °C.

$$\Delta L = \alpha \cdot L_0 \cdot \Delta T \tag{5.4}$$

In reference to a single pixel 0.9 μm give only 0.005 μm/px. Looking at Figure 5.16, a much greater apparent movement of the recorded targets is shown even during a smaller temperature change.

The above calculations for the CamCube (45 μm \* 204 px) result in an expansion of the sensor of 1.2 μm in total which is 0.006 μm per pixel.

Those small figures mean that the expansion of the sensor itself cannot be detected separately and is anyway negligible.

Nevertheless, the apparent movements of the targets are present as can clearly be seen in Figure 5.16 on the following page. This might be caused through a temperature dependent mounting of the imaging sensor. Maybe the housing or other internal parts are not expanding equally.

If an thermal expansion coefficient for the aluminium housing of around  $23.5 \cdot 10^{-6}$  is assumed, this means that one side of a camera with an original length of roughly 6 cm is then increased by 70  $\mu\text{m}$ . Considering the greater heating of the back of the CamCube on one side (see. Fig. 5.1), this could result in a slight rotation of the sensor of about 0.3 mgon.

The analysis of movement of the calculated target centers was carried out as described in the methods chapter on page 22. The repeatability is given in Figure 5.15. Also prior experiments with the old mounting of the SR3000 showed the same movement pattern.

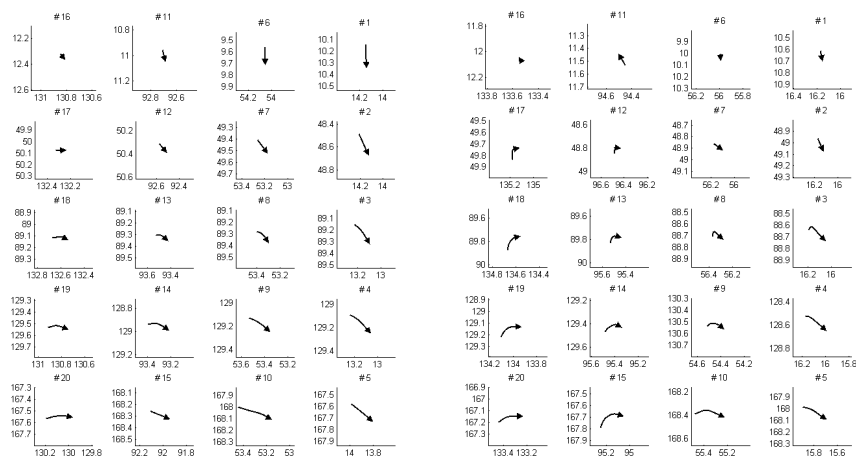
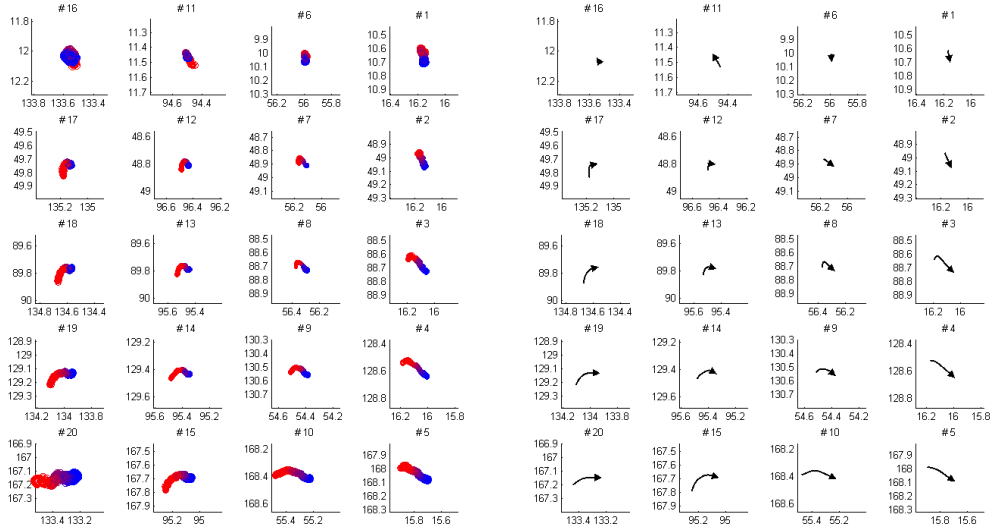


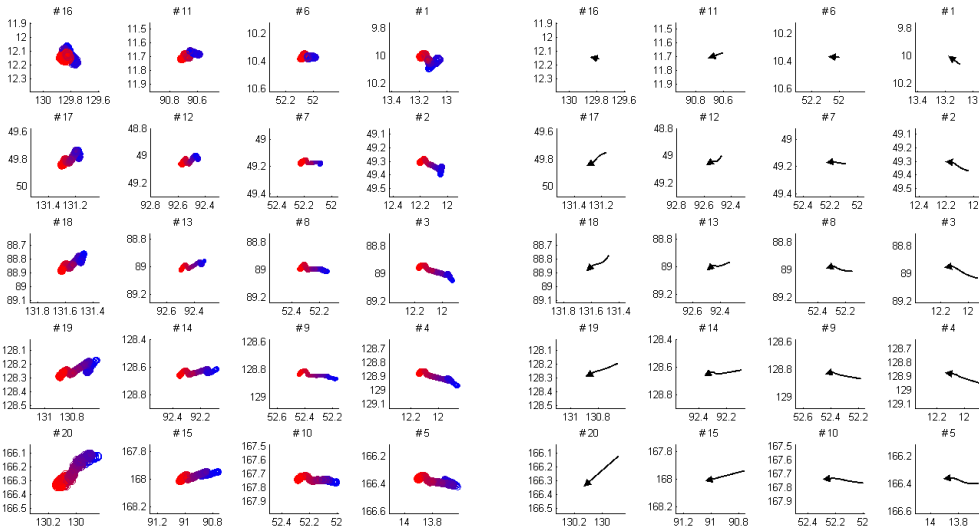
Figure 5.15: Repeatability of SR3000 Experiments. Two cooling down experiments.

<sup>3</sup>taken from the “Journal of Research of the National Bureau of Standards” Research Paper 2308, 1952

The diameter of the drawn target positions is related to the accuracy of the target determination. The colouring indicates the measured temperature. Vectors were drawn manually and should only be a help for visualisation.



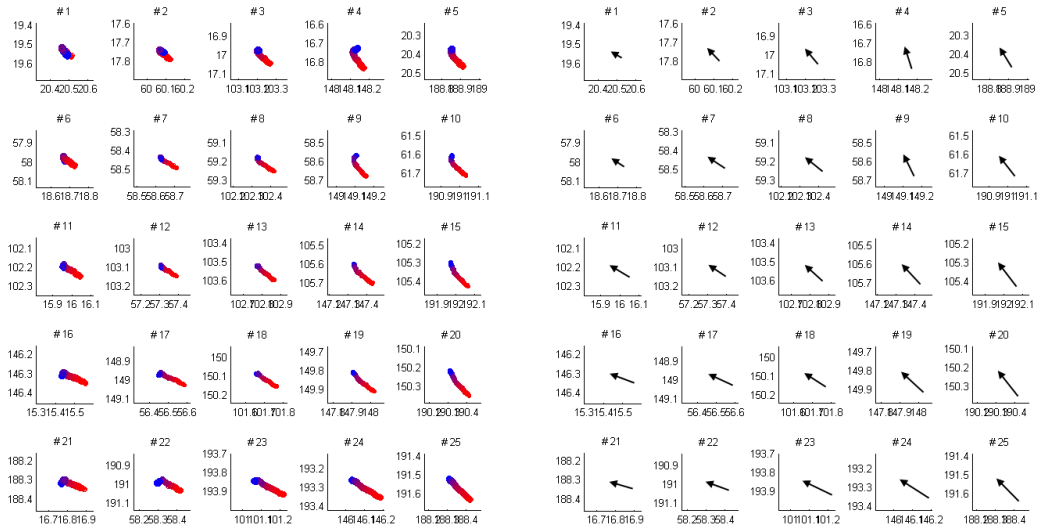
(a) Cooling down the SR3000.



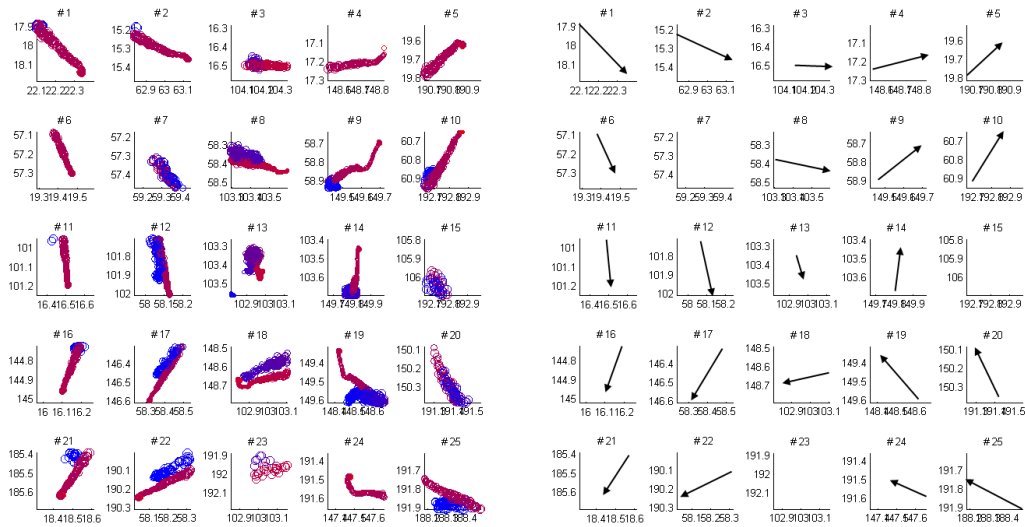
(b) Warming up the SR3000

Figure 5.16: Apparent movement of the steady targets recorded with the SR3000. The movements are of the same shape but in opposite directions if the temperature rises or falls.

The diameter of the drawn target positions is related to the accuracy of the target determination. The colouring indicates the measured temperature. Vectors were drawn manually and should only be a help for visualisation.



(a) Cooling down the CamCube.



(b) Warming up the CamCube.

Figure 5.17: Apparent movement of the steady targets recorded with the CamCube. In contrast to the results from the SR3000 the movements do not show the same behaviour for heating or cooling.

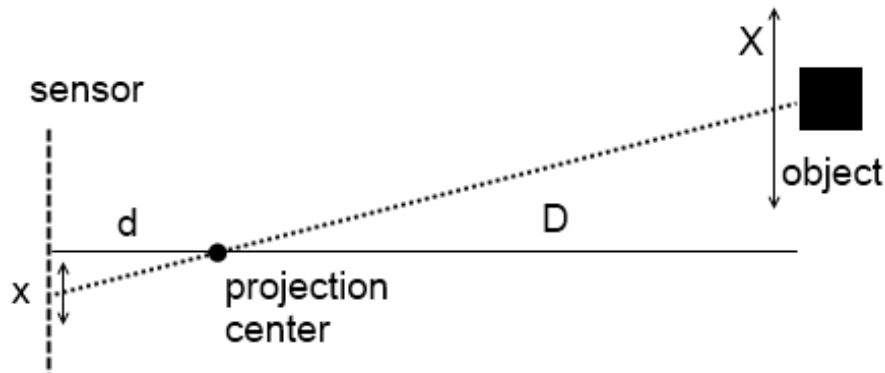


Figure 5.18: Principle of the projecting theorem.

$$\frac{x}{d} = \frac{X}{D} \quad (5.5)$$

Values that reasonably resemble the set-up of the experiments with one meter distance, a movement of the target of 0.2 pixels in each direction and averages of 43  $\mu\text{m}$  pixel size together with 10 mm focal distance are assumed. Applying those numbers to the projecting theorem (Formula 5.5), those movements result in errors of about 1.2 mm in the object room and are therefore not negligible for some applications.

A closer look at the internal structure would be interesting and would probably reveal some construction problems. The registered movements could be avoided or at least reduced by changing the layout of the instrument-internal mounting.

### 5.3.3 Sensor-location dependence of dark current

To see the spatial dependence of dark current within the sensor, five pixels were chosen and closer examined. Four of them were chosen in the corners and one in the middle of the sensor (see Figure 5.19). Each pixel was placed between the tiles used for target recognition. This should assure that not pixels within a target circle are sampled when experiments with uncovered lens and the target pattern used in this work are examined.



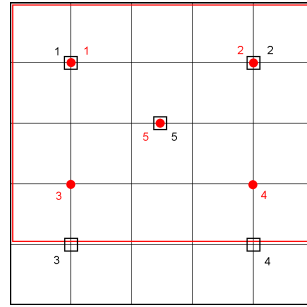


Figure 5.19: Placement of the sampling points. (black squares: CamCube, red circles: SR3000)

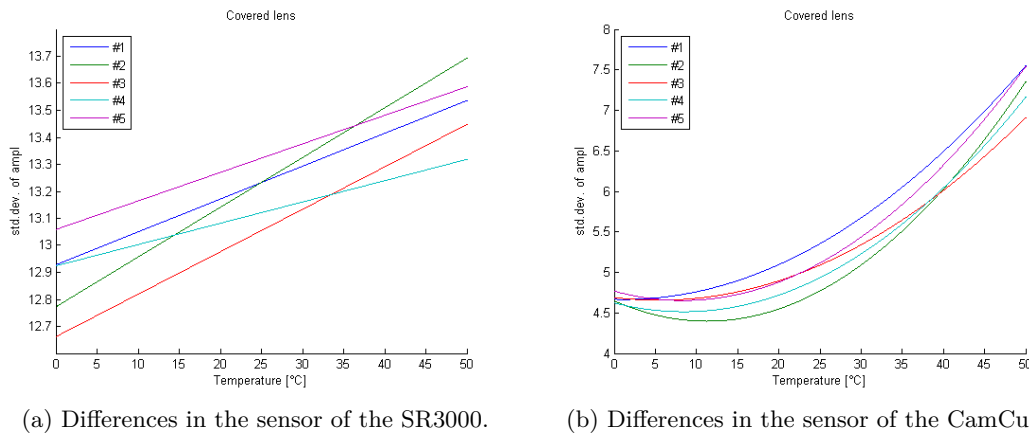


Figure 5.20: Behaviour of dark current dependent on the location of the pixel of interest.

The results depicted in Figure 5.20 show certain trends. While the standard deviation calculated with 10 values of the dark current amplitudes of the SR3000 could be well fitted with a linear trend the CamCube’s data needed a quadratic function. Both cameras have larger deviations of amplitudes at higher temperatures as expected.

A closer look at the amplitude data of the SR3000 reveals that the slope of pixels in the left part of the sensor are greater than the ones in the right part aside from pixel number two.

The standard deviations derived from the CamCube show that pixels in the left part are most of the time larger than the other ones. This is consistent with the findings in chapter 5.3.1 on page 36. It must not be forgotten that the used housingtemperature might not be directly related to the temperature of the sensor.

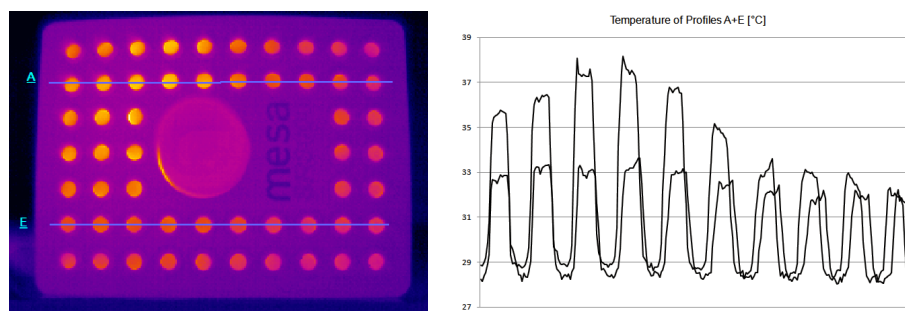
### 5.3.4 Influence on the active Illumination

It was expected that during operation the illumination would heat up until a certain point and also change its behaviour according to that elevated temperature. To tackle this Rapp (2007) recommends more efficient light sources which seems to be an obvious solution.

It is not known exactly which type of LEDs are used for the cameras but assuming similar properties like for a GaAs-IR LED with a central wavelength of 950 nm a temperature coefficient of the radiation power of  $-0.55\%/K$  is stated in Gluiber et al. (1993). This means that an increasing temperature causes decreasing illumination power. For the temperature range that is covered in this work ( $50\text{ }^\circ\text{C}$ ) this means a decrease of  $27.5\%$ . The amplitudes of the derived data do show such a correlation, which can be seen in Figure 5.7 for the SR3000 and in Figure 5.8 for the CamCube.

Furthermore, the temperature coefficient of the forward voltage coming to the LEDs is stated as major influence. Due to the fact that the cameras were not disassembled, this could not be further investigated.

A change of temperature or supply voltage is seen as time delay causing influence via a change of the signals' bandwidth that cannot be distinguished from the actual measurement. This time delay translates into a phase shift by  $\varphi = 2\pi f_{mod}\tau$  (Oberhauser, 2006). To be able to assess this influence the temperatures of the LEDs are needed. It was possible to get thermal images of the LEDs of the SR3000 because they were not behind a filter like the ones of the CamCube. The camera was left in standby until no major change of its temperature occurred and images were taken as in Figure 5.21.



(a) Thermal image of the SR3000 front (b) Profiles A+E through the LEDs.  
Increased temperature can be seen in the top left corner of the image. Differences up to  $5\text{ }^\circ\text{C}$  were detected.

Figure 5.21: Infra red image of the SR3000s' LEDs in standby.

It was noticed that the temperature in one corner of the instrument was higher than in the other parts without obvious reason. Turning the instrument upside down did not change the unequal temperature distribution. Close-ups through the vents finally revealed some chips to be the heat source (Fig. 5.22). According to Oggier (2011) this is caused by drivers which heat up because of the high Frequency they are working at. More background information about LED driving circuits can be found in chapter 2.3.1. in Gluiber et al. (1993).

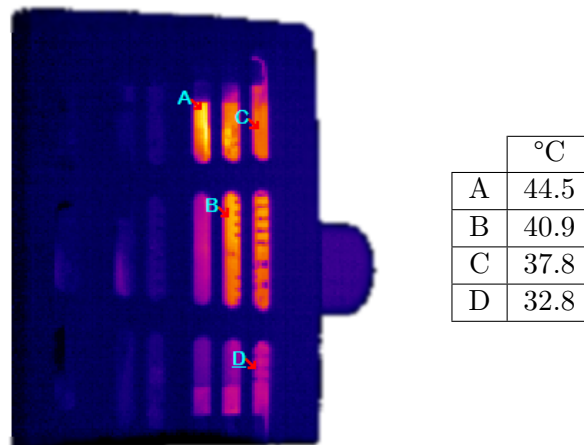


Figure 5.22: Chips right behind the LED board.

The measurement of the LEDs of the CamCube was not possible because of the filter in front of them. Nevertheless the heat distribution, which was already measured punctually (see Figure 5.1 on page 27), agree with the recordings of the IR-camera.

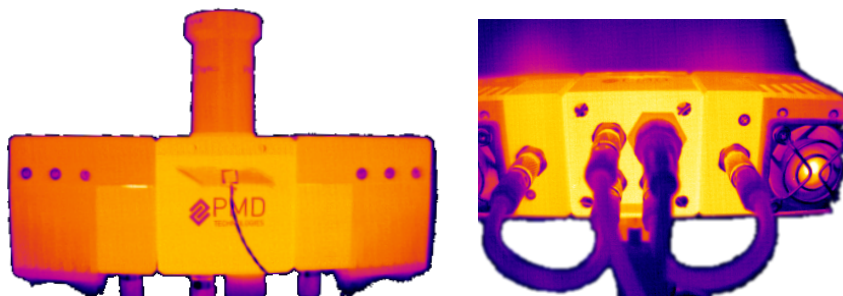


Figure 5.23: Infra red image of the CamCube during operation.

In the background of the right image in Figure 5.23 there is noticeable heating of the target due to the close distance to the illumination. Further research using the IR camera was not possible due to limited access.

### 5.3.5 Frequency Stability of the Illumination

The interesting Frequency for phase measuring principles is the modulation frequency of the carrier wave, which has to be stable. Not only the phase shift caused by the distance itself may occur but also phase shifts induced by the LED driving circuit, the LEDs itself (see above) and the receiving circuit that can not be distinguished (Gluiber et al., 1993).

A modulator is used to change the amplitude at a certain frequency provided by an oscillator. This results in darker and lighter sequences. The oscillator is expected to vary its frequency according to temperature and age. Depending on the Type of oscillator used, the accuracy is in the range of  $\pm 1$ -2.5 ppm. Additionally, the ageing effect usually reduces the frequency by about 1 ppm per year. Those effects can be minimized by calibration and the use of an internal temperature sensor mentioned in R ueger (1990). If a non-compensated room temperature crystal oscillator (RTXO) is assumed with a typical stability of  $\pm 2.5$  ppm within a temperature range of 0 to 50 °C, this results in  $\pm 200$  Hz using 80 MHz as reference Frequency.

The Frequency of the system's master clock is mentioned to be 80 MHz for the first range-cameras built by LANGE (2000). This is also the case for the newer SR3000 (Oggier, 2011). If a frequency stability of  $\pm 2.5$  ppm is assumed as mentioned above the resulting distance uncertainty can be calculated with formula 5.6. The factor from the master clock frequency (80MHz) to the actual modulation frequency (20MHz) is 4 (Lange, 2000). This leads to a resulting distance uncertainty of 0.15 mm:

$$\Delta s_{ref} = s_{max} - s_{min} = \frac{c_0}{2} \left( \frac{4}{f_{ref}(1 - 2.5ppm)} - \frac{4}{f_{ref}(1 + 2.5ppm)} \right) = 0.15 \text{ mm} \quad (5.6)$$

Calculating the other way round, a change of 6.67 kHz would be necessary to change the distance by 5 mm.

With the help of PAUL BERLINGER from the "Institute of Applied Physics" an IR-Sensor was built based on circuits published in Gray et al. (1998). A detailed list of parts can be found in chapter A.1.3 on page 54.

Figure 5.24 shows a scheme of the final set up of the experiment.

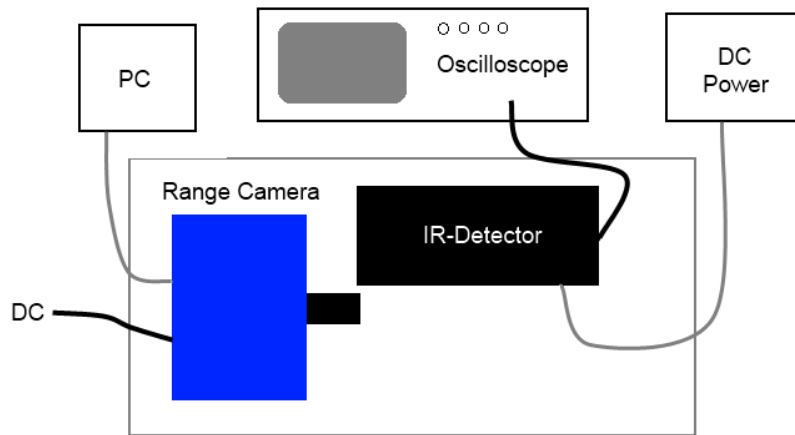


Figure 5.24: Set up of the frequency-counting experiment.

Considering a modulation frequency of 20 MHz, the signal should be sampled with at least 40 MHz following Nyquist’s sampling theorem. The Oscilloscope’s capacity of saving 2500 sampling points at once and the interval of interest suggested a timescale of the oscillator of 1  $\mu$ s. This scale turned out to be ideal to show other features of the signal like a small pre-burst peak depicted in Figure 5.25 below.

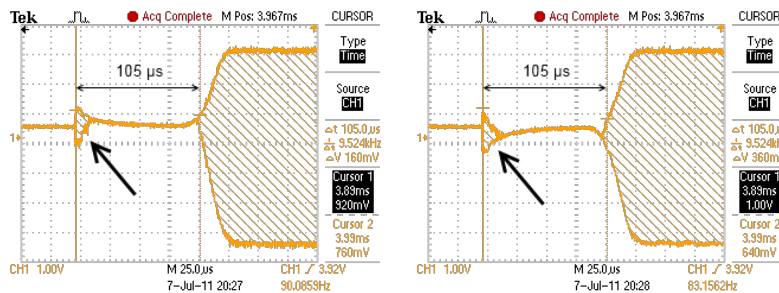


Figure 5.25: Plots showing small peaks occurring constantly 105  $\mu$ s before the main burst of the SR3000. This is caused by the cameras’ electronics and does not influence the actual measurement.

This peak always occurs around 105  $\mu$ s prior to the main burst, which lasts for the chosen integration time. According to Oggier (2011), this is an unwanted effect caused by settling effects of the driver-/illuminations-electronics interaction.

A look at the FFT results of several captured signals of the SR3000 shows an increasing power of the 20 MHz peak according to temperature. The large jump at 35  $^{\circ}$ C within the

data is most likely related to the ventilation of the SR3000 working on a higher level (see Figure 5.26).

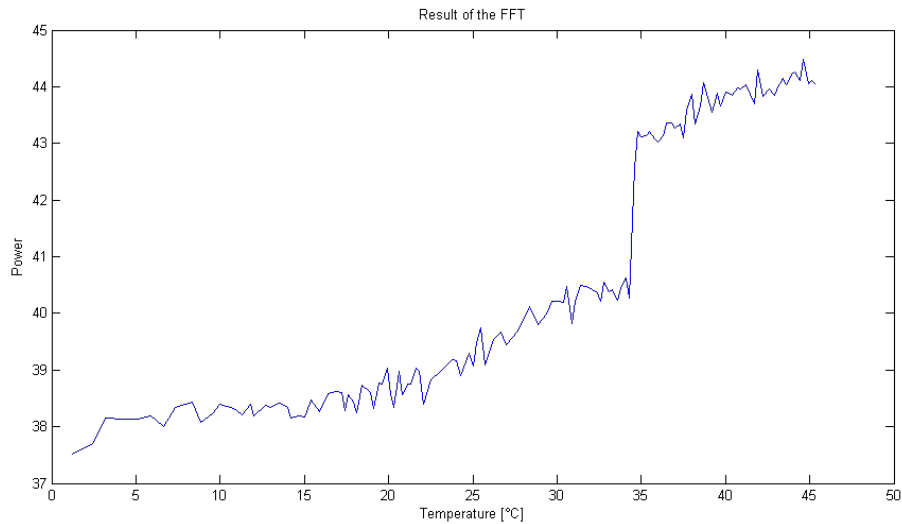


Figure 5.26: Powers of the 20 MHz main frequency of the SR3000 plotted against the temperature of the sensor.

Unfortunately the methods used for the determination of the modulation frequency were not advanced enough to reveal a change of frequency.

## 5.4 Summary of Results

All experiments were carried out with a distance of about one meter between the camera and the target's surface. The summary is given in the following table (Table 5.3).

Experiment	SR3000	CamCube
distance (warming)	1.4 $\frac{mm}{^\circ C}$	4 $\frac{mm}{^\circ C}$
distance (cooling)	2.1 $\frac{mm}{^\circ C}$	
standard deviation of measured distance (warming)	0.038 $\frac{mm}{^\circ C}$	2.8 $\frac{mm}{^\circ C}$
standard deviation of measured distance (cooling)	0.027 $\frac{mm}{^\circ C}$	
amplitude (warming)	-38.8	-6.9
amplitude (cooling)	-52.9	-8.6

Table 5.3: Overview of the results.

The results summarised in the table above show basic differences between both cameras.

The fact that the SR3000 switches on its ventilation at a certain level makes it necessary to characterise the two states separately. In most experiments carried out with the SR3000 the behaviour during the range from the start until the ventilation reaches its maximal r.p.m. could not be interpreted.

Although the gradients of the CamCube are larger than the ones of the SR3000 they do not need to be split and could therefore be easier taken into account for corrections.

The large differences in the slope of the amplitudes reflect the different approaches of combining illumination and filtering.

# 6 Conclusion

## 6.1 Conclusions

It was found that temperature was influencing several different parts of range cameras. A more detailed research on each of the topics visited in this work could be done to further deepen the understanding of all temperature related effects.

The main problem seems to be the different behaviour of the drivers of illumination and sensor as a small delay already causes noticeable distance differences (see Figure 6.1). The solution was the introduction of a reference path realised with an optical fibre leading directly from the illumination unit to a part of the sensor (Heinol, 2001; Kahlmann, 2007; Oggier, 2008).

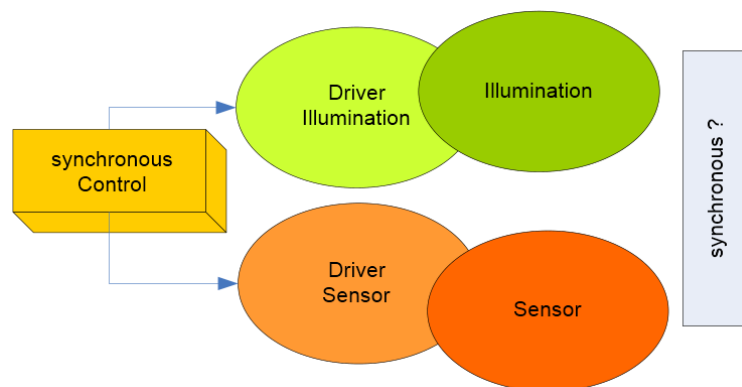


Figure 6.1: Temperature and ageing effects are stated as main influences for loss of synchronisation. (Image taken/translated from Oggier (2008)) Different behaviour of sensor and illumination drivers at certain temperatures are blamed for losing their synchronism.



## 6.2 Temperature related recommendations for practical work

The use of the cameras at constant temperatures is an obvious way to avoid correcting the data afterwards. This however is hardly realistic due to the fact that the temperatures of the environment, the housing, the sensor, the illumination and the electronics have to be at a steady state. Switching on and starting the measurement fairly in advance of the final observations turned out to be really helpful. This way switch-on effects did not have to be considered.

A note in Rüeiger (1990) states that the lifetime of GaAlAs diodes could be 10 times longer at 25 °C compared to operation at 50 °C. Also a drop of the emitting power to 75% after 10 000 hours (more than a year) use at room temperature is mentioned. This implies that continuous operation at elevated temperatures should be avoided to reduce unnecessary stress on material.

In respect to the oscillator, operation at a steady temperature is preferred, however not obligatory because temperature does not have a great impact on it (see Chapter 5.3.5).

Finally it should be thought of the possibility of condensation water when working at quickly changing environments.

## 6.3 Future Work

Previous works that use the integration time as base e.g. for their correction algorithms might be revisited to check if the use of temperature data related on that integration time might be more appropriate.

More detailed Experiments with the use of an appropriate climate chamber should be carried out. Thereby not only measurements at certain temperature levels should be taken but rather during changing temperatures to be able to differentiate between heating and cooling effects. As final result a hysteresis of the heating and cooling effects on the measurements is expected.

# A Appendix

## A.1 Instruments used for Experiments

Apart from the cameras and the PC for recording following instruments were used:

- Heating and cooling devices
- Data-Logger for recording the meteorology of the measurement laboratory
- Temperature-Logger for monitoring the temperatures of both cameras

### A.1.1 Devices for heating and cooling

For reasons of convenience and because of the unavailability of a proper climatic chamber, everyday life devices present at the Institutes were used. Prior to the experiments it was made sure that they could reach all temperatures needed by a series of tests.

#### Oven

The oven used for heating up the cameras is a simple miniature baking oven. To avoid irregular warming by radiant heat, two shieldings of black cardboard with the side pointing away of the heaters covered with aluminium foil were built in to ensure a much smoother rise and smaller variations of the temperature. The temperature differences inside the oven were found to be around 2 °C and therefore in an acceptable range. For reasons of security in respect to the cameras the maximum temperature was set several degrees below the highest allowed storing temperature.

#### Refrigerator

The ice box of a refrigerator was used to cool down the cameras below 0 °C. The cameras were protected against direct cold airflows by a cardboard wall. Furthermore a thermal insulation was introduced between the carton and the frigistors.

## A.1.2 Temperature Loggers

### Meteorology-Data-Logger

The ambient room temperature was monitored with a PCE-THB 40<sup>1</sup> thermohygrometer and barometer. Temperature humidity and pressure were recorded every five minutes. Recordings starting at the end of December 2010 show only small variations of the temperature. More details can be found in Chapter 3.4.

### Temperature Logger

For the recording of present temperatures a 4-channel Thermo-Data-Logger was used, which was in this case the PCE-T 390 with a temperature range of -100 °C up to more than 1000 °C. The accuracy of  $0.1\text{ °C} \pm (0.4\% + 0.5\text{ °C})^2$  and a time resolution of up to a second were seen to be suitable for the measurements. Also the reaction time of around a second should not pose a problem.

Nevertheless, it turned out to be necessary to check the recorded data for erroneous temperature as well as equal timestamps following each other and hindering the automated analysis. While the erroneous temperature values were interpolated, the problem with the timestamps was tackled within the analysis routine by keeping only the first unique timestamp.

### Temperature Sensors

Two K-Type wire sensors that were delivered with the Temperature-Logger were used to tune the oven and the cooling unit to the desired temperatures. An additional K-Type magnetic surface probe (thermo-electra<sup>3</sup> Model: 80513) was used to determine the temperature of the cameras. For the determination of the surface temperature of the CamCube (see Fig. 5.1) a thermo-electra surface probe (80102A) was used.

## A.1.3 Instruments for Illumination Analysis

### IR-Detector

To be able to detect the Modulation frequency of the illuminations, a sensitive receiver was necessary. A circuit similar to the ones described in Gray et al. (1998) was developed and constructed by PAUL BERLINGER.

<sup>1</sup><http://www.industrial-needs.com/measuring-instruments/thermo-hygrometers.htm>

<sup>2</sup>precision tested by the manufacturer at  $23 \pm 5\text{ °C}$  (PCE Instruments, 2010)

<sup>3</sup><http://www.thermo-electra.com/>

The main parts were an IR-Photodiode (Centronic Silicon Photodetector AEPX-65) with 2.4 ns response time and a wideband precision operational amplifier (Burr-Brown OPA620).

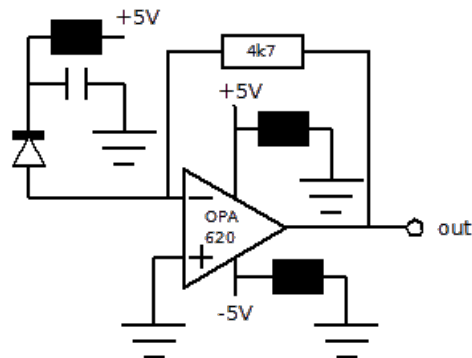


Figure A.1: Schematic sketch of the circuit used to build the IR sensor.

One of the available current supplies had a fixed output of 5.25 V but luckily the other one was adjustable and was set to the same voltage.

## Oscilloscope

The used oscilloscope was lent from the EMCE. It was a Tektronix TDS2022B 2-channel instrument. It was fast enough for determining the modulation frequency of the active illumination.



Figure A.2: 4-channel oscilloscope similar to the one used. (from the Tektronix manual: "TDS1000B and TDS2000B Series Digital Storage Oscilloscopes")



# Bibliography

- Besl, Paul J. (June 1988). “Active, optical range imaging sensors”. In: *Machine Vision and Applications* 1.2, pp. 127–152. ISSN: 0932-8092. DOI: [10.1007/BF01212277](https://doi.org/10.1007/BF01212277). URL: <http://www.springerlink.com/index/10.1007/BF01212277>.
- Bureau International des Poids et Mesures (2006). *Le Système international d’unités*. 8th. 1. Paris: STEDI MEDIA. ISBN: 92-822-2213-6. URL: [http://www.bipm.org/utils/common/pdf/si\\_brochure\\_8\\_en.pdf](http://www.bipm.org/utils/common/pdf/si_brochure_8_en.pdf).
- Frey, Jochen (2008). *Bildsensorik mit Tiefgang - Stand der PMD-Technik, Roadmap und Perspektiven*. Tech. rep. Siegen: PMD Technologies GmbH. URL: [http://spectro.net.de/portals/visqua/story\\_docs/vortraege\\_2008/081118\\_pmd\\_visionday/081118\\_01\\_frey\\_pmd\\_technologies.pdf](http://spectro.net.de/portals/visqua/story_docs/vortraege_2008/081118_pmd_visionday/081118_01_frey_pmd_technologies.pdf).
- Gluiber, W. et al. (1993). *Optische Abstandsmessung*. Haus der Technik - Fachbuchreihe. Essen: R. Pepperl.
- Gray, Malcolm B. et al. (1998). “Photodetector designs for experiments in quantum optics”. In: *Rev. Sci. Instrum.* Pp. 1–10. URL: [http://www.atom.fysik.lth.se/QI/laser\\_documentation/Selected\\_articles/Photodetector designs for Experiments in Quantum Optics.pdf](http://www.atom.fysik.lth.se/QI/laser_documentation/Selected_articles/Photodetector designs for Experiments in Quantum Optics.pdf).
- Heinol, Horst G. (2001). “Untersuchung und Entwicklung von modulationslaufzeitbasierten 3D-Sichtsystemen”. PhD thesis. University of Siegen. URL: <http://www.zess.uni-siegen.de/cms/diss/2001/heinol/heinol.pdf>.
- Kahlmann, Timo (2007). “Range imaging metrology: Investigation, calibration and development”. PhD thesis. ETH Zurich. DOI: [10.3929/ethz-a-005465562](https://doi.org/10.3929/ethz-a-005465562). URL: <http://e-collection.ethbib.ethz.ch/view/eth:41869>.
- Kahlmann, Timo, Fabio Remondino, and Hilmar Ingensand (2006). “Calibration for Increased Accuracy of the Range Imaging Camera Swissranger”. In: *Proc. of IEVM XXXVI.4*, pp. 136–141. URL: <http://citeseerx.ist.psu.edu/viewdoc/download?doi=10.1.1.62.8904&rep=rep1&type=pdf>.
- Karel, Wilfried (2007). “Range Imaging: 3D-Punktwolken in Echtzeit”. In: *Österreichische Zeitschrift für Vermessung und Geoinformation* 4, pp. 1–12.
- Karel, Wilfried, Sajid Ghuffar, and Norbert Pfeifer (2010). “Quantifying the Distortion of Distance Observations Caused by Scattering in Time-of-Flight Range Cameras”.

- In: *ISPRS XXXVIII*. URL: <http://www.isprs.org/proceedings/XXXVIII/part5/papers/228.pdf>.
- Lange, Robert (2000). “3D time-of-flight distance measurement with custom solid-state image sensors in CMOS/CCD-technology”. PhD thesis. University of Siegen. URL: <http://dokumentix.ub.uni-siegen.de/opus/volltexte/2006/178/>.
- Lange, Robert and Peter Seitz (Mar. 2001). “Solid-state time-of-flight range camera”. In: *IEEE Journal of Quantum Electronics* 37.3, pp. 390–397. ISSN: 00189197. DOI: 10.1109/3.910448. URL: <http://ieeexplore.ieee.org/lpdocs/epic03/wrapper.htm?arnumber=910448>.
- Luan, Xuming (2001). “Experimental Investigation of Photonic Mixer Device and Development of TOF 3D Ranging Systems Based on PMD Technology”. PhD thesis. University of Siegen. URL: <http://www.zess.uni-siegen.de/cms/diss/2001/luan/luan.pdf>.
- Lyon, K. G. et al. (1977). “Linear thermal expansion measurements on silicon from 6 to 340 K”. In: *Journal of Applied Physics* 48.3, pp. 865–868. ISSN: 0021-8979. URL: [http://ieeexplore.ieee.org/xpls/abs\\_all.jsp?arnumber=5103488](http://ieeexplore.ieee.org/xpls/abs_all.jsp?arnumber=5103488).
- Mesa Imaging (2006). *SwissRanger SR-3000 Manual*. Zürich. URL: [http://aiweb.techfak.uni-bielefeld.de/files/SR3000\\_manual\\_V1.03.pdf](http://aiweb.techfak.uni-bielefeld.de/files/SR3000_manual_V1.03.pdf).
- (2008). *SR-3000 Data Sheet*. Zürich. URL: [http://www.mesa-imaging.ch/pdf/SR3000\\_Flyer\\_Jan07.pdf](http://www.mesa-imaging.ch/pdf/SR3000_Flyer_Jan07.pdf).
- Möller, Tobias et al. (2005). *Robust 3D Measurement with PMD Sensors*. Tech. rep. Zürich. URL: <http://citeseerx.ist.psu.edu/viewdoc/download?doi=10.1.1.132.5821&rep=rep1&type=pdf>.
- Oberhauser, Klaus (2006). “Opto-Electronic Integrated Correlation Receivers for Time-of-Flight Based Distance Measurement Systems”. Dissertation. Vienna University of Technology. URL: <http://www.ub.tuwien.ac.at/diss/AC05033224.pdf>.
- Oggier, Thierry (2008). *3D-Bilderfassung in Echtzeit mit modernen hochintegrierten 3D-Kameras*. Stuttgart.
- (Aug. 2011). *personal communication*.
- Oggier, Thierry et al. (2005). “Swissranger SR3000 and First Experiences based on Miniaturized 3D-TOF Cameras”. In: *Proceedings of the First Range Imaging Research Day at ETH Zurich*. URL: <http://j-clavis.co.jp/pdf/h-4.pdf>.
- Otepka, Johannes (2004). “Precision Target Mensuration in Vision Metrology”. PhD thesis. Vienna University of Technology. URL: <http://media.obvsg.at/AC04346920-2001>.
- Pattinson, Timothy (2010). “Quantification and Description of Distance Measurement Errors of a Time-of-Flight Camera”. MA thesis. University of Stuttgart. URL: <http://>

- [//www.lulu.com/items/volume\\_68/8652000/8652310/1/print/distance\\_error\\_s\\_tof\\_camera-1.pdf](http://www.lulu.com/items/volume_68/8652000/8652310/1/print/distance_error_s_tof_camera-1.pdf).
- PCE Instruments (2010). *Manual: Digital Thermometer PCE-T 390*. Durham. URL: <http://www.industrial-needs.com/manual/manual-pce-t390.pdf>.
- PMD Technologies (2009). *Datasheet: PMD[vision] CamCube 2.0*. Siegen. URL: [http://www.pmdtec.com/fileadmin/pmdtec/downloads/documentation/datasheet\\_camcube.pdf](http://www.pmdtec.com/fileadmin/pmdtec/downloads/documentation/datasheet_camcube.pdf).
- Rapp, Holger (2007). “Experimental and Theoretical Investigation of Correlating TOF-Camera Systems”. PhD thesis. University of Heidelberg. URL: <http://www.ub.uni-heidelberg.de/archiv/7666/>.
- Ringbeck, Thorsten and Bianca Hagebecker (2007). “Dreidimensionale Objekterfassung in Echtzeit - PMD Kameras erfassen pro Pixel Distanz und Helligkeit mit Videoframerate”. In: *AVN*, pp. 263–270.
- Rüeger, Jean M. (1990). *Electronic Distance Measurement: An Introduction*. 3rd. Berlin; Heidelberg: Springer, p. 266.
- Schneider, Bernd (2003). “Der Photomischdetektor zur schnellen 3D-Vermessung für Sicherheitssysteme und zur Informationsübertragung im Automobil”. PhD thesis. University of Siegen. URL: <http://dokumentix.ub.uni-siegen.de/opus/volltexte/2005/43/>.
- Steiger, Oliver, Judith Felder, and Stephan Weiss (2008). “Calibration of time-of-flight range imaging cameras”. In: *Image Processing, 2008. ICIP 2008. 15th IEEE International Conference on*. IEEE, pp. 1968–1971. URL: [http://ieeexplore.ieee.org/xpls/abs\\_all.jsp?arnumber=4712168](http://ieeexplore.ieee.org/xpls/abs_all.jsp?arnumber=4712168).
- Trassinellia, M. et al. (2005). “Characterization of the geometry of an array of CCD pixel detectors”. In: *International Conference on Exotic Atoms and Related Topics*. Vienna, pp. 343–348. URL: [http://www.austriaca.at/0xc1aa500d\\_0x000fd4f7.pdf](http://www.austriaca.at/0xc1aa500d_0x000fd4f7.pdf).
- Weyer, Christoph A. et al. (2008). “Extensive metric performance evaluation of a 3D range camera”. In: *ISPRS 37.1*, pp. 939–944. URL: [http://www.isprs.org/proceedings/XXXVII/congress/5\\_pdf/163.pdf](http://www.isprs.org/proceedings/XXXVII/congress/5_pdf/163.pdf).
- Zach, Gerald, Milos Davidovic, and Horst Zimmermann (2010). “A 16 times 16 Pixel Distance Sensor With In-Pixel Circuitry That Tolerates 150 klx of Ambient Light”. In: *Solid-State Circuits, IEEE Journal of* 45.7, pp. 1345–1353. URL: [http://ieeexplore.ieee.org/xpls/abs\\_all.jsp?arnumber=5492315](http://ieeexplore.ieee.org/xpls/abs_all.jsp?arnumber=5492315).



# List of Figures

2.1	Overview of distance measurement principles. . . . .	4
2.2	The two range cameras used for the experiments. . . . .	6
2.3	Image sensors of the range cameras. . . . .	7
2.4	SR3000 and CamCube arrangement of LEDs. . . . .	8
2.5	Principle of burst-mode illumination. . . . .	9
2.6	Comparison of bursts of SR3000 and CamCube. . . . .	9
2.7	Timing schedule of the SR3000. . . . .	10
2.8	Detail of the first moments of a burst (CamCube). . . . .	11
2.9	Cooling of the SR3000. . . . .	12
2.10	Cooling of the CamCube. . . . .	13
3.1	Multipath effect in a corner. . . . .	14
3.2	Typical amplitude-image and target accuracies. . . . .	15
3.3	Metal platform on top of the tripod. . . . .	16
3.4	Range cameras with metal sheets for temperature tapping. . . . .	17
3.5	Check of steadiness of the Support. . . . .	18
3.6	Targets recorded by the SR3000 during 5 h. . . . .	19
3.7	Temperature in the Lab. . . . .	20
3.8	Final set up. . . . .	21
4.1	Data recording with both cameras and harmonisation. . . . .	22
4.2	Merging of data from experiments. . . . .	23
4.3	Getting rough target positions in MATLAB. . . . .	23
4.4	Calculation of the normal vector of an amplitude image. . . . .	24
5.1	Temperature distribution of the CamCube. . . . .	27
5.2	(SR3000) Sensortemperature vs. distance. . . . .	28
5.3	(SR3000) Housingtemperature vs. distance. . . . .	29
5.4	(SR3000) Housingtemperature vs. sensortemperature. . . . .	30
5.5	(CamCube) Housingtemperature vs. distance . . . . .	31
5.6	(CamCube) Housingtemperature vs. std.dev. of distance. . . . .	32
5.7	(SR3000) Temperature vs. amplitudes. . . . .	32
5.8	(CamCube) Housingtemperature vs. amplitude. . . . .	33
5.9	(CamCube) Housingtemperature vs. std.dev. of amplitudes. . . . .	34

5.10	Temperature of the sensor related to the chosen integration time. . . . .	35
5.11	Temperature dependence of dark current. . . . .	37
5.12	Dark current amplitude distribution of the SR3000. . . . .	38
5.13	Dark current amplitude distribution of the CamCube. . . . .	38
5.14	Temperature dependence of dark current. . . . .	39
5.15	Repeatability of experiments. . . . .	40
5.16	(SR3000) Apparent movement of targets. . . . .	41
5.17	(CamCube) Apparent movement of targets. . . . .	42
5.18	Principle of the projecting theorem. . . . .	43
5.19	Placement of sampling points. . . . .	44
5.20	Behaviour of dark current dependent on the location of the pixel. . . . .	44
5.21	(SR3000) Thermal image of the SR3000. . . . .	45
5.22	(SR3000) Chips right behind the LED board. . . . .	46
5.23	(CamCube) Thermal image of the CamCube. . . . .	46
5.24	Set up of the frequency-counting experiment. . . . .	48
5.25	(SR3000) Small peaks before the main burst. . . . .	48
5.26	(SR3000) Powers of the 20 MHz main frequency of the SR3000. . . . .	49
6.1	Loss of synchronism due to temperature and ageing. . . . .	51
A.1	Circuit of the IR-sensor. . . . .	55
A.2	4-channel oscilloscope similar to the one used. . . . .	55

Figure 2.2a on page 6 created by “PMDTech” is licensed under „CC-by-sa 3.0/de“.<sup>4</sup>

---

<sup>4</sup>see <http://creativecommons.org/licenses/by-sa/3.0/de/legalcode> for details

## List of Tables

2.1	Storage- and operating-temperatures. . . . .	13
2.2	Focal lengths and modulation frequencies of the cameras. . . . .	13
5.1	Temperatures of the CamCube in standby. . . . .	26
5.2	Safety limits $t_s$ for a two-tailed statistical security $S$ of 95 % depending on the redundancy $k$ . . . . .	34
5.3	Overview of the results. . . . .	50

# Curriculum Vitae

PHILIPP ZACHHUBER, born 25.08.1984 in Wels, Austria

Volunteering paramedic since 2004. Ambulance driver since 2005. Permission for working full-time as paramedic since 2006.

## Education:

- 2009-2011 Master "Survey and Land Registration"
- 2008-2009 ERASMUS Year Abroad: "University College London" (UCL)
- 2005-2008 Bachelor "Geodesy and Geomatics Engineering"<sup>5</sup>
- 1999-2004 Federal Higher Technical Institute for Civil Engineering "HTL 1 Linz"
- 1995-1999 Grammar school "BRG-Steyr"
- 1991-1995 Primary school Bad Hall

## Work Experience: Numbers in brackets = working weeks

1. (4) Swietelsky Bauges.m.b.H
2. (8) Vermessungsbüro Dipl.-Ing. Walter Höllhuber
3. (4) Alpine Mayreder Bau GmbH
4. (9) OÖ Boden- und Baustoffprüfstelle GmbH
5. (5) OÖ Boden- und Baustoffprüfstelle GmbH
6. (4) Vermessungskanzlei D.I. Rudolf Schöffmann
7. (5) Vermessungskanzlei D.I. Rudolf Schöffmann
8. (6) Österreichische Bundesforste AG
9. (2) Österreichisches Rotes Kreuz, LV OÖ
10. (4) Österreichische Bundesforste AG
11. (8) Deutsches Zentrum für Luft- und Raumfahrt
12. (2) Österreichisches Rotes Kreuz, LV OÖ
13. (6) Vermessungskanzlei D.I. Rudolf Schöffmann
14. (12) Leica Geosystems

---

<sup>5</sup>Thesis: "Investigation of correlations between coordinates from the 'Austrian Federal Forests' and the land surveying office"